

Article

The Effect of Unsupported Sleepers/Bearers on Dynamic Phenomena of a Railway Turnout System under Impact Loads

Mehmet Hamarat ¹, Mayorkinos Papaelias ², Mika Silvast ³ and Sakdirat Kaewunruen ^{1,*} 

¹ Department of Civil Engineering, School of Engineering, The University of Birmingham, Birmingham B152TT, UK; mzh670@bham.ac.uk

² School of Metallurgy and Materials, The University of Birmingham, Birmingham B152TT, UK; m.papaelias@bham.ac.uk

³ Loram Finland Oy, Yliopistonkatu 58 D, 33100 Tampere, Finland; mika.a.silvast@loram.com

* Correspondence: s.kaewunruen@bham.ac.uk

Received: 26 February 2020; Accepted: 24 March 2020; Published: 28 March 2020



Featured Application: The new findings highlight for the first time the nonlinear dynamic phenomena of turnout systems considering unsupported composite and concrete sleepers and bearers. The in-depth insights stemmed from multi-body simulations of dynamic train—turnout interaction demonstrates the influences of unsupported sleepers on dynamic responses, load redistributions, dynamic impact factors and wheel/rail contact forces. The novel insights can be used (not limited to) as a reference for the design, inspection and maintenance of railway switches and crossings.

Abstract: Track settlement is a common problem observed in ballasted railway tracks. The ballast bed and the material layers underneath it, deform under repeated trainloads and create uneven support conditions along the track. In some cases, the ballast settlement could be detrimental and the sleepers lose contact with the ballast bed partially or completely, resulting in higher contact forces and load distributions over the supported sleepers. Numerous studies have been conducted to investigate the phenomenon for normal tracks. Nevertheless, railway turnouts are somehow neglected. As a consequence, this study focuses on the relation between unsupported sleepers/bearers (particular name for turnouts) and a railway turnout system to develop the understanding of the response of turnout system under dynamic loadings. A 3D Finite Element Method (FEM) model is inherited from previous study and adopted to reflect the cases with unsupported bearer configurations. It is noteworthy that inherited model is capable of reflecting the impact forces, which is an inherent and fundamental characteristic of a railway turnout. Model verification is done with the parent model that was verified by field measurements. Three different support conditions (i.e., one, two, three unsupported bearers), five different velocities and six different positions of unsupported bearers are simulated. The results show that the performance of ‘fibre-reinforced foamed urethane’ (FFU) bearers are promising and more, unsupported bearers carry significant loads at particular locations, which is contrary to the sleepers on normal track that are subjected to insignificant loads.

Keywords: railway; turnout; switches and crossings; impact forces; unsupported sleepers; unsupported bearers

1. Introduction

In railway applications, if the track is ballasted, the role to support track systems is widely played by a ballast layer, so-called ballast bed. It is composed of crushed and graded rock particles providing

high friction to absorb the energy produced by dynamic forces owing to train–track interactions, and adequate strength to support track system. In ideal case, it is assumed that the ballast layer is laid uniformly along the track, which secures constant support forces for the track via sleepers, and a natural drainage. In reality, tracks are exposed to environmental effects leading to progressive deterioration in the ballast bed. In this sense, a well-known process is ‘mud pumping’ that is associated with ballast fouling due to foreign particles, filling the voids inside the ballast bed and inhibiting the drainage. The process changes the mechanical properties of the ballast bed and induces more volatile dynamic forces that incur track settlements, which accumulate mud pumping. This cascade of events repeat perpetually and eventually, terminates in a failure of the ballast bed that cannot provide any support for the sleepers/bearers. In that case, sleepers/bearers lose the contact with the ballast bed, which amplifies the wheel-rail contact forces and increases risks for safety. This phenomenon is also known as ‘hanging sleepers’.

Numerous studies have been conducted to understand the effect of unsupported sleepers on dynamic behavior of track components, and train–track interaction. In a pioneering study, it has found that a significant difference between dynamic response of a supported track and a track with unsupported sleepers occurs at a frequency of 200 Hz at which sleepers are likely to have a considerable movement. The situation could be more critical at pinned-pinned frequency owing to greater dynamic strains for the track with unsupported sleepers [1]. Most importantly, the ballast is a primary source of damping, in the absence of which vibration of unsupported sleepers are almost undamped, and consequently, strains in components of the unsupported sleepers are expected to be higher and result in lower component life [1]. In fact, the phenomenon is more sophisticated as sleepers could be partially supported in various forms. The type and length of void under partially supported sleepers influence the natural frequencies and occasionally, cause a “mode swapping” [2].

Only effective option to investigate various forms of void under unsupported sleepers seems to be the numerical modeling, as well as fully unsupported sleepers. Other options such as in-situ and laboratory measurements present a great challenge in terms of a methodology and a suitable experimental setup due to the nature of ballast bed deterioration where the forming process does not follow the same pattern in each case. It is believed that a well-calibrated numerical model with in-situ or laboratory measurements could represent the real track with a good precision. The calibration is strongly related to the level of numerical modeling. For instance, it has found that a quasi-static analysis underestimates the contact forces in comparison to a dynamic analysis for unsupported sleepers [1]. Likewise, a model of a simple mass on a Hertzian spring could largely neglects the dynamic effects of train–track interaction [3]. Apart from the level of a numerical model, it should be noted that the calibration is also sensitive to environmental conditions during measurements. In an experiment with a 1/5 scale experimental setup, it was observed that the outcome of the experiments were diverging at higher frequencies [4]. Similar problem was observed in [1] when they made measurements on frozen ballast bed.

Admittedly, higher level of numerical modeling complicates the solution process. Nevertheless, it gives an advantage that more advance numerical models enable researchers to investigate the unsupported sleepers for various scenarios. In [5], a 3D Finite Element Method (FEM) model with solid elements was developed to study the effect of the gap under the unsupported sleepers (one or two sleepers unsupported in their work) together with vehicle velocity; to assess the track settlement with a specific formula based on the output of the simulation. The results show that ballast/sleeper contact forces are gradually amplified over the adjacent sleepers with respect to height of the gap and velocity, whereas it becomes zero for the track section with unsupported sleepers. In case of two unsupported sleepers, the gap could be closed and some contact forces could be produced [5]. Similar conclusions were obtained in [6] in which they expanded the ranges of parametric values and differently, used a 3D numerical model with two rails and a vehicle. By contrast, their study also shows that local maxima could be observed in different configurations considering the number of hanging sleepers, vehicle speed and the height of gap configurations. In another study [7], by means

of configuration, several scenarios for a one-sided partially unsupported sleepers was simulated and resulted in similar conclusions such that higher speed increase the contact force variations. They also show that the effect of triangular configuration, where three assumed voids are sequentially placed under left, right and then left rails, have no significant effect on the contact forces. In another study, the effect of sleeper spacing on the dynamic response of the system is found significant for partially and fully supported sleepers [8]. The larger sleeper bays escalate the rail displacement for both partially and fully unsupported sleepers. Similarly, it is shown in a recent study that the rail displacement was escalated for different number of axles, so-called bogie patterns and axle loads [9].

Surprisingly, researchers have avoided taking advantage of numerical analysis to investigate the unsupported sleepers/bearers over a turnout, a complex structured component on a railway track to divert traffic from one route to another one. More importantly, turnouts have an inherent asymmetrical topology (Figure 1) that increases the likelihood of occurrence of unsupported bearers. Only few researches have been encountered in the literature [10,11]. They show that turnouts also suffer from voided sleepers/bearers and can amplify the contact forces up to four times high. Nevertheless, these models mostly consider static or quasi-static loading, the insufficiency of which is mentioned previously. Furthermore, a single bearer was considered and analyzed in those studies, which was assumed to be sufficient to represent the behavior of whole turnout structure. Nevertheless, it was shown in [12] that the sleepers/bearers are subjected to different loading conditions based on their length and location along a turnout.

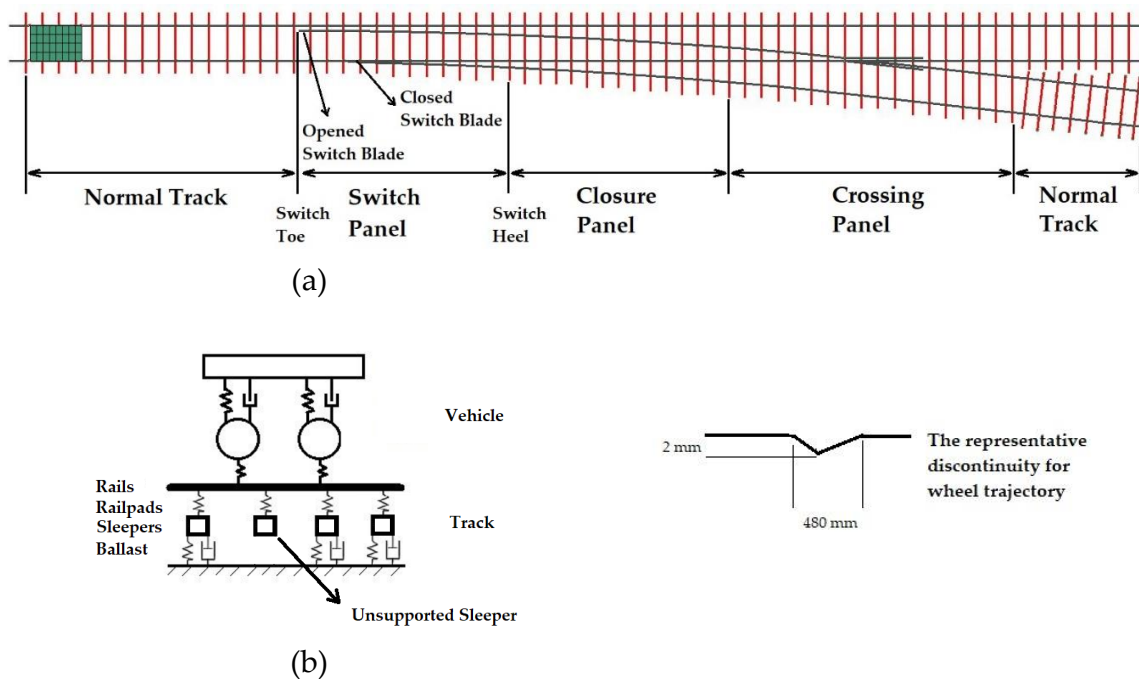


Figure 1. The FEM model. (a) The layout of a standard turnout and (b) the schematic vehicle–track couple.

Briefly, it seems that the effect of unsupported sleepers/bearers over a turnout have been investigated insufficiently with reference to above studies. Hence, the aim of this study is to analyze the response of a turnout system with unsupported sleepers/bearers via a more sophisticated numerical model that is capable of capturing dynamic forces. Various scenarios are adopted in numerical process such as one, two and three sleepers/bearers hanging with respect to different vehicle speed.

2. Numerical Model

A numerical model of a standard turnout with a crossing angle 1:9 and an equivalent rail profile of 54E1, which is adapted from [12], is used to investigate the dynamic effects of unsupported bearers. For clarity, the term ‘bearer’ is used instead of ‘sleeper’ in the following sections, where a bearer means a specific longer sleeper for turnouts. Equivalent profile is preferred to facilitate the calculations with parallel to downgrading the numerical reflection of the geometry of turnout from 3D solid model to 3D beam model. A simulation of a 48-meter turnout with a full geometry, so-called 3D solid model, is also possible but is believed to be not feasible as it consumes a lot of effort and time regarding available technology. A coupling strategy between two numerical methods, such as finite element model and multi-body simulations, is adopted here. The scope of the study is to consider the nonlinear dynamic responses of the coupling train-track and train-turnout systems, which leads to simplification of the vehicle geometry as a spring-mass system. The coupling tool between the two methods is provided by Hertzian contact theory. Figure 1 shows a descriptive model of a turnout.

In the numerical model, rails and bearers are modeled with beam elements in contrast to rail pads, ballast and subgrade, where spring-dash-board is applied. It is assumed that the process leading to unsupported bearers is finished, meaning that the bearers are fully unsupported or namely hanging. In other words, there is no contact between bearers and ballast bed. To consider no-contact situation, the spring-dash-board elements representing ballast bed and substructure under the unsupported bearers are removed from numerical model. This strategy is applied separately for every scenario where the location of unsupported bearer changes.

Generally, materials properties of the authors’ numerical model in [12] have been re-applied in this study. The slight difference is that a turnout with FFU bearers has been found be promising in terms of performance [13–15] and is considered in this study to gain further insights into the dynamic behaviors of a turnout system with FFU bearers as a case study. The model has 77 bearers with varying lengths from 2.4 m to 4.7 m. The bearer spacing is 0.71 m on average. They are connected to rails via a fastening system, which, in reality, consists of fishplates, bolts, rail pads and clips but here, is represented by springs considering the elasticity provided by rubber rail pads. The stiffness of rail pad is in the range of practical applications, 1300 kN/mm. The damping properties of rail pad is neglected based on [16] which indicates that the effect of rail pad damping is limited when compared to an overall damping of a track having a well-compacted ballast bed. In the simulation, the concept of “beam on an elastic foundation” is used where ballast and subgrade is represented by series of spring-dampers. The stiffness and damping properties of ballast bed are 45 kN/mm and 32 Ns/mm per normal bearer. Additionally, those properties of ballast bed per bearer are adjusted with respect to bearer length. The earth on which the subgrade and ballast bed are laid is assumed rigid and therefore, one end of spring-dash boards are fixed as a boundary condition. On the other hand, track components are free to move or rotate on their vertical planes. By taking advantage of multibody simulation, the car body of a rolling stock is downsized to spring mass system. Furthermore, the vehicle is modeled as a single bogie due to more significant contribution of wheel mass into dynamic response of the track–train system in comparison to car body. The bogie consists of bogie frame and two wheelsets, where the mass per wheelset is 20 tons, and they are connected to each other by spring-dashboards acting as primary suspensions. The vehicle moves in facing direction on trough route of the turnout. Moreover, it travels a 45 m distance at a constant speed ranging from 10 to 50 m/s during both wheelsets on the track. The speed values are approximately minimum and maximum admissible speed in the UK [17]. The boundary conditions enable the vehicle to move in longitudinal and vertical direction; to rotate around lateral (pitch motion) and longitudinal axis (roll motion). Finally yet importantly, properties of the numerical model are presented in Table 1.

Table 1. Dynamic material properties used in the numerical model [12].

Element	Type	Number of Elements	Properties	Value
Rail	Beam	1980	ρ^1	7800
			E^2	210
			PR ³	0.3
Bearer	Beam	3070	ρ^1	740
			E^2	8.1
			PR ³	0.25
Rail Pad	Spring	245	k^4	1300
Ballast	Spring/Damper	5900	k^4	45
			c^5	32
			k^4	1.15
Primary Suspension	Spring/Damper	8	c^5	2.5

¹ Density (kg/m³). ² Modulus of elasticity (GPa). ³ Poisson Ratio. ⁴ Stiffness (MN/m). ⁵ Damping coefficient (kNs/m).

As aforementioned, the coupling between track and vehicle is provided by Hertzian contact theory. According to this theory, it is assumed that contact forces are a product of contact stiffness and elastic deflection, where contact stiffness between two geometries is related to modulus of elasticity (E), Poisson ratio (ν), load (Q), and the radii of surfaces of geometries (R). In general, the load is accepted as a static load to facilitate the calculation. Assuming rail and wheel have infinite radius in one direction (then, radii of surfaces for wheel and rail are R_{wheel}, R_{rail} respectively), an analytical formula for contact stiffness is derived for railway applications [18]. Introducing this contact stiffness into the Hertz formula gives Equation (1). It should be noted that elastic deflection is predicted as an imaginary penetration between nodes in numerical calculations, which equals the distance between wheel (δ_w) and rail nodes that also contain the information of track surface roughness ($\delta_r + \delta_{ir}$).

$$F = \sqrt[3]{\frac{3E^2Q\sqrt{R_{wheel}\cdot R_{rail}}}{2(1-\nu^2)^2}} \times (\delta_w - \delta_r - \delta_{ir}) \tag{1}$$

Track surface roughness in the formula is obtained by field measurements and applied in the simulation to reflect realistic conditions. A roughness profile for 48 m turnout is obtained from [12]. The profile was extracted from 28 measurements for 30-km track length and represents worst track conditions regarding maximum mean and standard deviations. It is noteworthy that rail surfaces have no surface irregularities, perfectly smooth with the exception of a small irregularity at crossing nose representing the geometrical discontinuity (Figure 1).

An explicit time integration used for the calculations in this study is well-known for its effectiveness on dynamic problems when large displacements or impact forces are of interest. It inherently provides stability, namely convergence, during solution process. Furthermore, in this study, the solution process is enriched with a dynamic relaxation [19] that ensures the vehicle and track is in an equilibrium before the calculation. Otherwise, the vehicle would bounce on the rails due to gravitational forces caused by small gaps between rails and wheel, which would produce artificial vibrations. Another challenge while using an explicit time integration is to decide the time step for the simulation that depends on the length of an element. Here, the same time step in [12] is preferred to obtain high quality results and acceptable computer clock time for the computation.

Model verification is conducted by comparing the current model with the parent model in [12]. It provides flexibility and more importantly, facilitates the verification process, which is quite complex for unsupported bearers due to inherent behavior of the ballast bed that exhibit different characteristic in every case. Therefore, a separate verification with field measurements is omitted. In [12], verification of the model was done based on two different measurements in the literature. Those measurements were based on two different methodologies, such as measuring the acceleration and measuring the contact forces. Acceleration method is simple to apply but insufficient to extract contact forces whereas

it is vice-versa for measuring the contact forces. It was believed that verification by two methods would be a cross validation. The parent model was found to be sufficient to represent the behavior of the turnouts under dynamic loading. The comparison for both models is given in Figure 2. The current model demonstrates similar contact profile, mostly. The part where the discrepancy emerges is the effect of unsupported bearer. Additionally, it also captures 250 Hz impact forces, namely P2 forces. The model, as well as parent model, has a limited ability to show the high frequency part of impact forces (P1). Practically, P1 forces are mostly ignored due to short duration. In conclusion, it is assumed here that the model having the similar contact force profile with the parent model is also sufficient to represent turnouts with unsupported bearers.

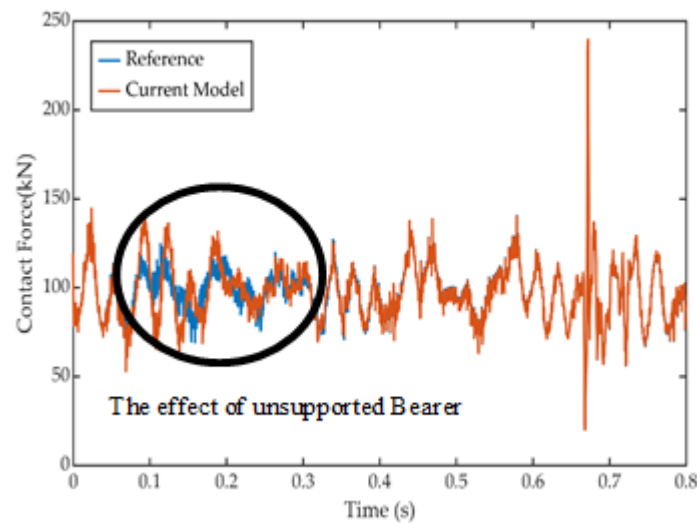


Figure 2. Comparison between the current model and parent model.

3. Results and Discussion

In this section, results of the simulation for three different scenarios, six different positions and five different velocities are presented. To increase the readability, 2D graphs are merged into 3D graphs and subsections are categorized based on the outcomes of the simulations. Furthermore, several new definitions are introduced not to repeat longer definitive sentences. When the word 'relative' is used, it indicates the difference between the results of unsupported bearers and reference case where all bearers of which are supported. Likewise, 'relative increase' indicates the ratio between relative value and reference case.

3.1. Vibration Response of the Bearers

Table 2 compares the natural frequencies of an FFU bearer, experimentally [20,21] and numerically. It should be noted that the bearer properties are adjusted to the one in the experiments while solving the natural frequencies since the length of the bearers in the current model is different from the experiment and a limited data on the FFU bearers. As indicated in Table 2, the numerical results seem to be consistent with the experimental ones. The maximum discrepancy between results is 13% at the third mode. In the experiment, the location of the springs that is used to provide free-free condition are not indicated, which is believed to be the origin of the increasing error through the higher modes. In other words, the discrepancy between two cases is inevitable. As a result, it could be assumed that experimental and numerical bearer models are similar and the discrepancy is acceptable. Using the same methodology, natural frequencies of a bearer under the crossing nose are estimated (Table 2). As can be seen from Table 2, the length of the bearer influences the natural frequencies significantly. Regarding the vibration theory, it is expected that impact forces over the crossing nose could excite the resonance frequencies of bearers, particularly unsupported bearers, due to high frequency high

magnitude impact forces. Hence, acceleration of rail seat close to impact location is analyzed in frequency domain.

Table 2. Natural frequencies of the bearer used in the model.

Mode No	FFU Bearer		FFU Bearer
	Experimental [20]	Numerical	Numerical
1	68	69	25
2	143	137	87
3	247	214	150
4	N/A	446	208
5	N/A	832	296
6	N/A	1030	445
7	N/A	1322	641
8	N/A	1850	870

In Figure 3, indications of resonance behavior could be detected. However, it seems that only first (37 Hz) and fourth (251 Hz) modes are excited below impact frequency. Several factors could lead to this result such as skipping some resonance frequencies quickly, contribution of random track surface causing noise in the signal or limitation in numerical method. It is noteworthy that the dominant frequencies are higher than natural frequencies of free-free condition due to the different boundary conditions. Furthermore, two peaks at higher frequencies result from track irregularities. For instance, the peak at 970 Hz is close to so called pinned–pinned frequency of track with the rail profile used in this study (54E1) [22].

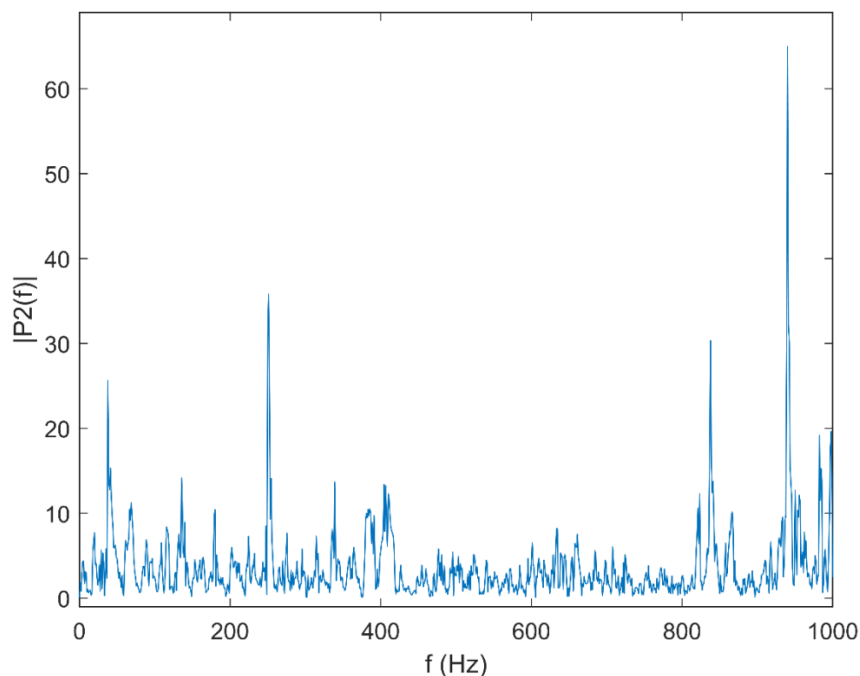


Figure 3. Fast Fourier Transform of acceleration at rail seat position under the crossing nose.

3.2. Bearer Displacement at Rail Seats

From Figures 4–9, maximum bearer displacements at rail seat location, associated with different vehicle velocities and three cases, are depicted for six different positions. As observed from Figures 4–9,

a distinctive difference results from the number of unsupported bearers for all cases. Expansion of unsupported track section can cause higher track deflection [4,8]. The magnitude of deflection is strongly related to unsupported bearer position due to varying track stiffness along the turnout. Highest deflections are observed when the shortest bearers, which are laid after longest bearer to adjust transition between normal track section and S&C, are unsupported. The relative increase of displacements in those cases could reach up to 86%, 224% and 467% for one, two and three unsupported bearers, respectively. On the other hand, the lowest deflections are mostly observed when the bearers at the closure panel are unsupported. Track stiffness is relatively higher along this zone due to larger surface contact area supported by ballast bed. This can also cause higher bending moments attributable to higher track stiffness [12]. The maximum bearer displacements for one, two and three unsupported bearers at closure panel have 53%, 115% and 198% relative increase.

In Figure 4, maximum displacement of unsupported bearers at normal track section is presented. The effect of vehicle velocity seems to have a limited impact on the maximum bearer displacement in different velocities, where one and two unsupported bearers are of interest. Nevertheless, it is perceptible that higher velocities cause higher bearer displacements on the occasion of three unsupported bearers. The maximum displacement of the middle bearer of three unsupported bearers increase 20%, when velocity goes from 10 m/s to 50 m/s. Similar findings are mentioned in [4] which demonstrates that three unsupported sleepers cause significantly higher sleeper displacements with parallel to vehicle velocities rather than one and two unsupported sleepers. It should be noted that one and two unsupported cases in [4] also suffer from slightly higher displacements with increased velocities, contrary to current study where track surface irregularities affecting significantly track–train interactions produce significant fluctuations in terms of sleeper displacement.

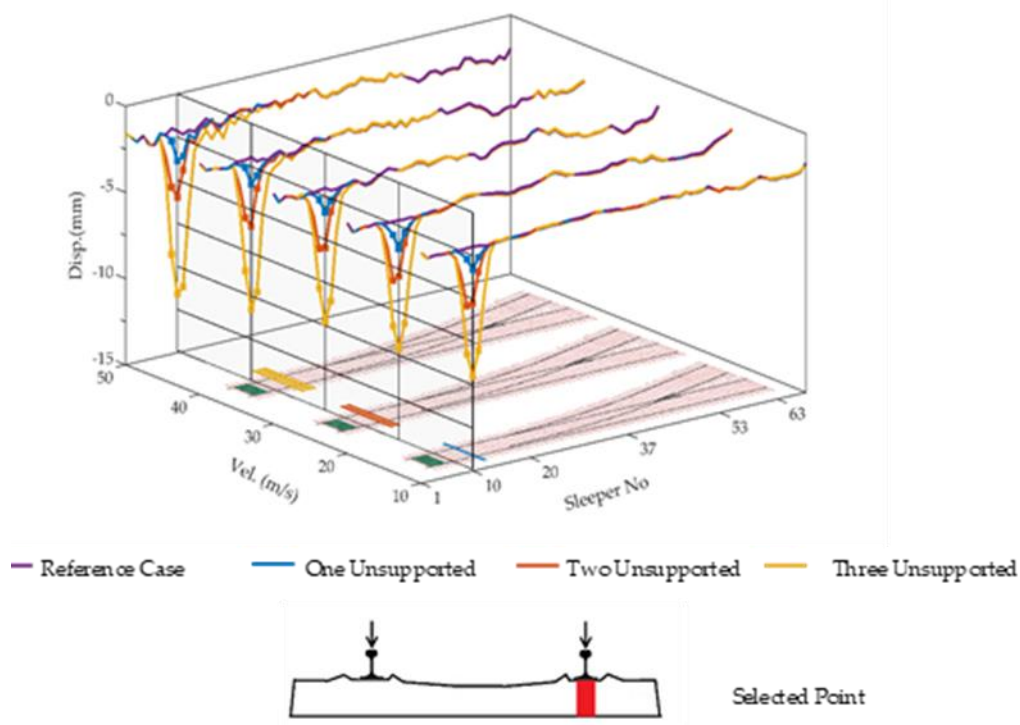


Figure 4. The maximum displacement of bearers at rail seats when an unsupported bearer exists at normal track section.

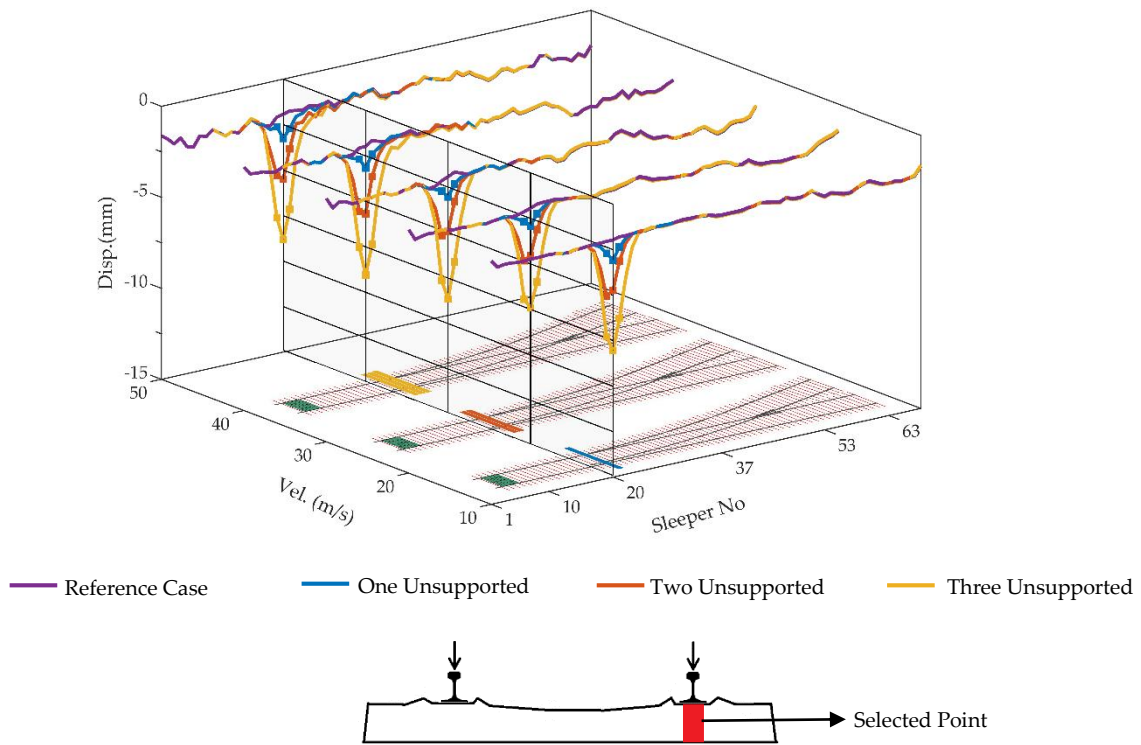


Figure 5. The maximum displacement of bearers at rail seats when an unsupported bearer exists under switch blade.

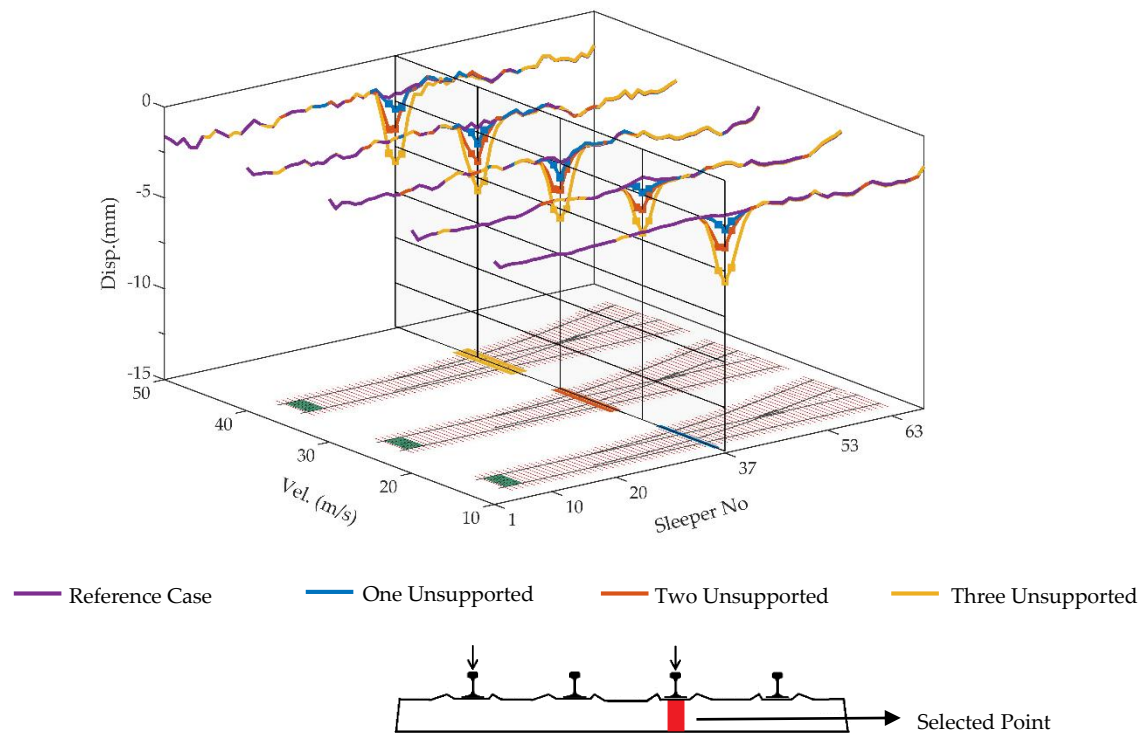


Figure 6. The maximum displacement of bearers at rail seats when an unsupported bearer exists at closure panel.

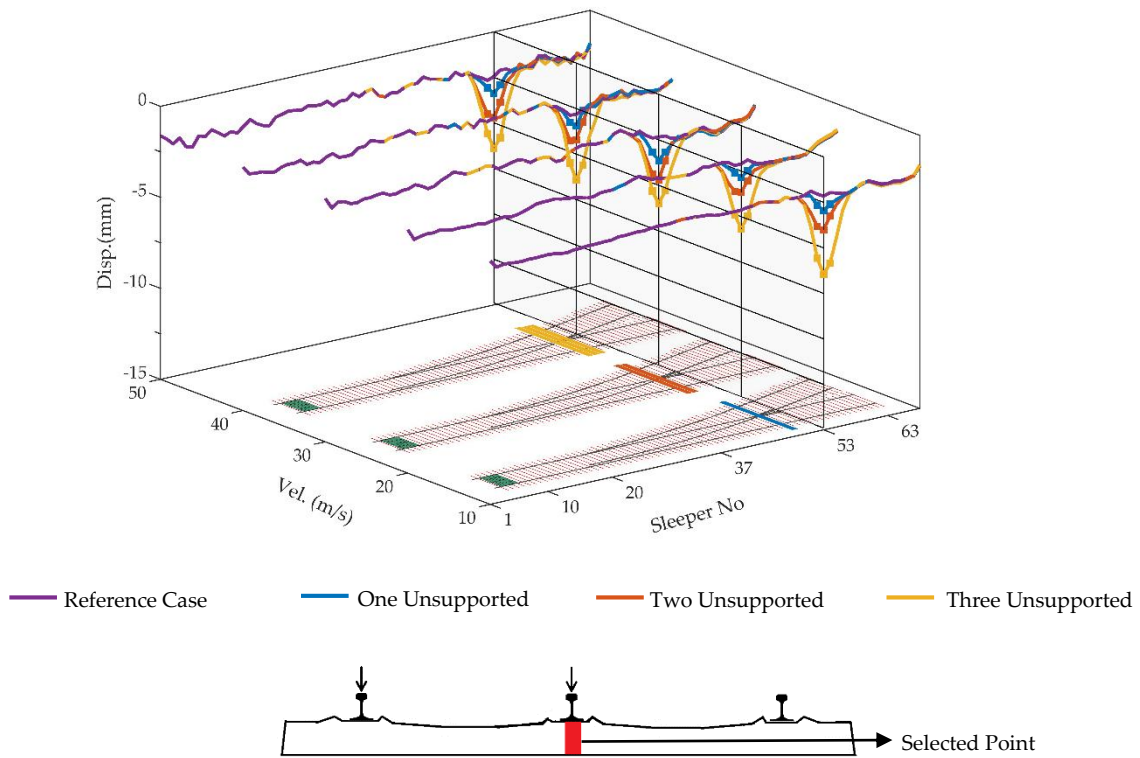


Figure 7. The maximum displacement of bearers at rail seats when an unsupported bearer exists under crossing nose.

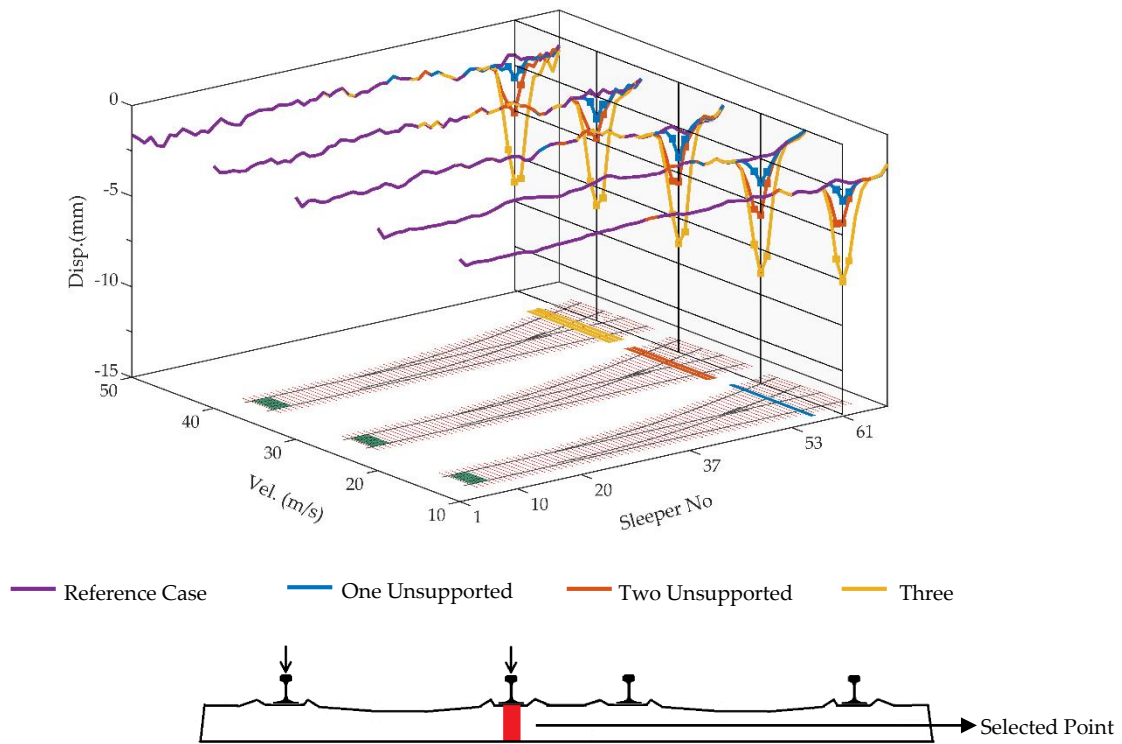


Figure 8. The maximum displacement of bearers at rail seats when the longest bearer is unsupported.

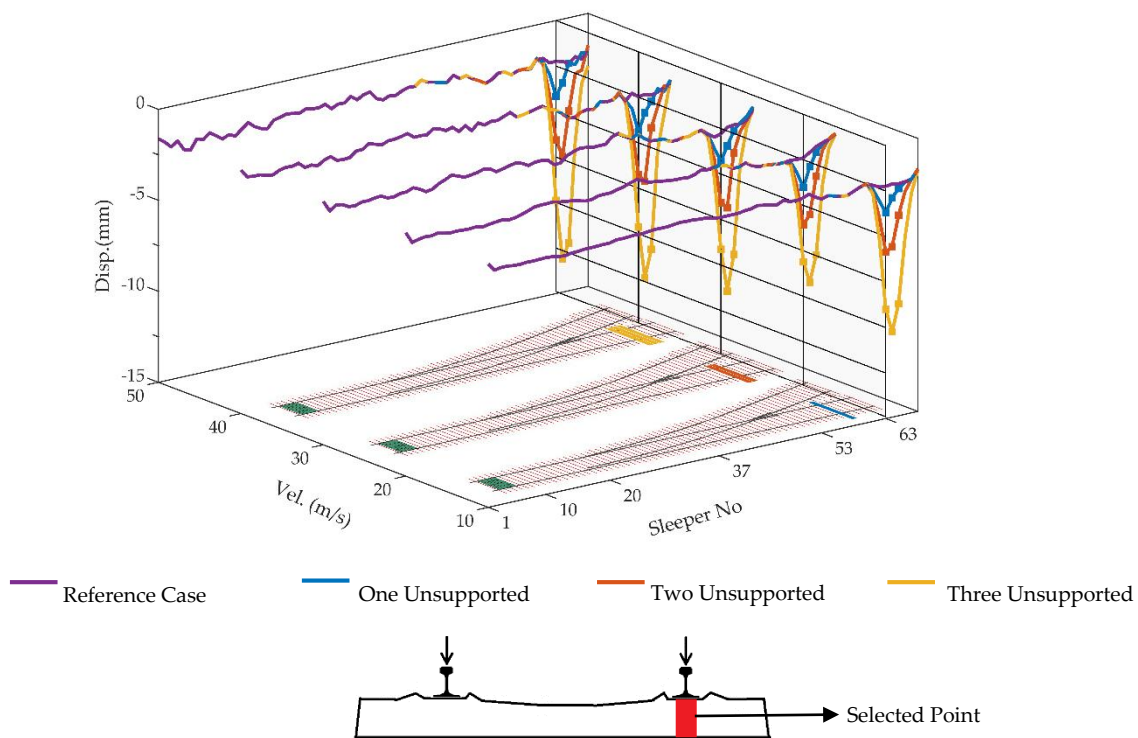


Figure 9. The maximum displacement of bearers at rail seats when the shortest bearer is unsupported.

The trend in normal bearers disappears for the unsupported switch panel bearers in Figure 5, despite having same bearer length with normal track section. Highest deflection is observed as 9 mm at 40 m/s for three unsupported bearer case. It is evident that switch blades can contribute significantly to track stiffness. In the figure, a perceptible decrease in the displacement value at 20 m/s is also believed to be a result of the dynamic response of the vehicle to track surface irregularities. This effect is obvious in the reference case as the higher velocities cause fluctuation on the result curve. In Figure 6, simulation outcomes for unsupported bearers at closure panel are given. Lowest maximum displacement values are mainly observed in this case. As aforementioned, track stiffness is relatively high at this section along the closure panel. The effect of different velocities is indistinct however, the number of unsupported bearer still have important effect. Among the deflection values, highest value is 5.87 mm for the case of three unsupported bearers with 50 m/s vehicle speed whereas the lowest displacement is 2.9 mm for one unsupported bearer at same speed. The corresponding value in the reference case is 2 mm of displacement. Similar behavior, occurs when the unsupported bearers emerge under the crossing panel (Figure 7) An interesting behavior could be realized in Figure 7. Although there is a trend of higher displacements with higher speeds, in general, three unsupported bearers do not fit that profile. For instance, the bearer displacements at 50 m/s compared to 10 m/s are higher for the reference, one and two unsupported cases. The differences are 0.3 mm, 0.4 mm and 0.7 mm, respectively. However, the displacement value for same condition is 0.1 mm less in the case of three unsupported bearer. It is apparent that three unsupported bearers enable a positive effect at 50 m/s. A similar behavior is found in [6] where the wheel-rail contact forces become stable subsequent to exceeding certain number of unsupported sleeper. The reason could be related to smooth transition between sleepers instead of sudden change. However, this positive effect could also be a result of limitation in the numerical model where the crossing nose is represented by beam elements.

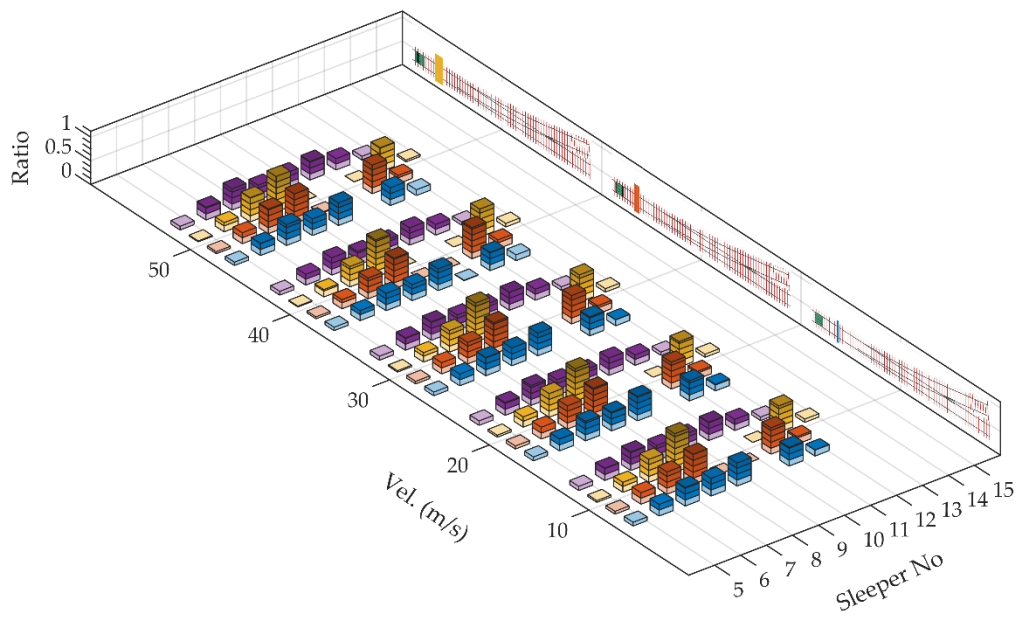
In Figure 8, the results of simulations for unsupported longest bearers and based on simulation case, unsupported shortest neighbor bearer are presented. In this case, the displacement values for longest bearers are higher when compared to bearers under crossing nose that are relatively in similar lengths. The section where the longest bearers are laid is close to physical separation point of two

tracks. Therefore, the dependency between two tracks seems to be weak; and results in slightly lower track stiffness. In the case of one bearer, maximum displacements occur at unsupported bearers for all velocities. Displacement values are 3.1 mm, 3.8 mm, 4.1 mm, 3.7 mm and 3.2 mm from 10 m/s to 50 m/s, which indicates that a resonance like behavior could be observed and critical speed could be 30 m/s. For other cases, similar pattern is observed but up to speed of 40 m/s. It is noted that analysis interval of velocity parameter might be insufficient to show resonance effect. Another outcome that could be perceived from the figure is that in the case of three unsupported bearers, one of the unsupported bearer is the shortest bearer (bearer no. 62) that shows recognizable displacement similar to longest bearer (bearer no. 61). Interestingly, the other unsupported bearer (bearer no. 60), which has similar length with longest bearer, does not deflect in similar order with longest bearer, even though it shows similar deflection in the case of two unsupported bearers. It can be found that shortest sleeper causes an asymmetrical loading.

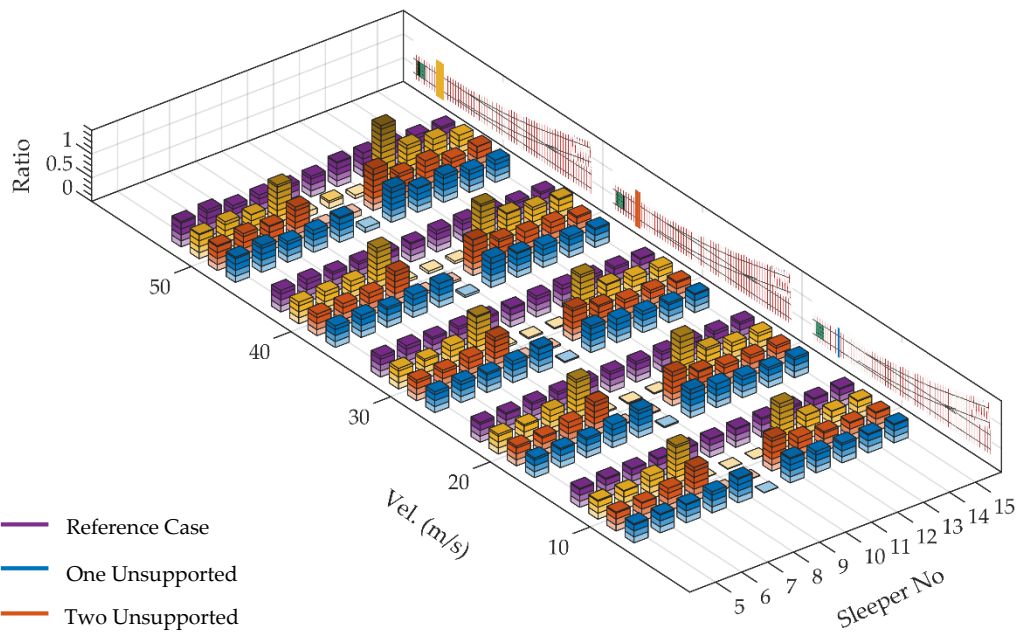
In Figure 9, deflections of unsupported shortest bearers are given. The effect of different velocity is obvious in three unsupported bearer case. Displacements of the bearer increase significantly from 10.3 mm to 13.1 mm with respect to velocity. A small decline at 20 m/s could be a result from any track surface irregularity or the sudden transition from the longest bearer to the shortest bearer. Similarly, higher velocities cause higher deflections in the case of two unsupported bearers. The effect of velocity is not clear for one unsupported bearer. As can be seen from the figure, maximum displacement occurs at the unsupported bearer in the middle, in the case of three unsupported bearers. Nevertheless, the maximum displacement could be observed on different unsupported bearers (maker positions show) with reference to different speeds in the case of two unsupported bearers, which is related to track irregularities.

3.3. Rail Seat Forces

In railway applications, the vehicle load is transferred via fastening system to bearers and then the ballast bed. In the absence of ballast support, the support conditions totally change in the vicinity of the unsupported bearers and the load transferred by fastening system change dramatically over unsupported bearers and adjacent bearers. In this section, uneven load distributions over the bearers are investigated based on the force transferred via fastening system. In Figure 10, the force transferred via fastening system/ rail seat force (named here for simplicity) is shown for unsupported bearers at normal track section. Four cases (i.e., one, two and three unsupported bearers and reference case) and velocities ranging from 10 m/s to 50 m/s are illustrated in the figure. The ratio is defined as rail seat force over static wheel load. The results show that the significant loss of force is obvious for the unsupported bearers, despite slightly escalation with higher velocities. On the other hand, forces increase for the fully supported adjacent bearers in all cases. In Figure 10b, the ratio ranges from 0.5 to 1.3. Furthermore, the relative increase could be as much as 32%/33%, 77%/75% and 130%/134% higher for former/latter adjacent bearers of one, two and three unsupported bearers at speed of 10 m/s. This conclusion indicates that such an outcome as indicated in [5], which was that the sleeper next to the unsupported sleeper in travelling direction is most subjected to increasing dynamic forces, could be inaccurate. Furthermore, it shows the number of unsupported bearer has a considerable effect on the load distribution. The worst is the case where three bearers are unsupported, which is 1.3 times higher than static load. It is noteworthy that the ratio is 0.5 in reference case under same condition. In contrast to number of unsupported bearers, the effect of different velocities is unclear. The irregularities seem to be decisive on the load distributions. For instance, relative increase from 10 m/s to 50 m/s, is 32%/33%, 35%/36%, 25%/27%, 24%/37% and 24%/39% for former/latter adjacent bearers of one unsupported bearers. Similar results are obtained for adjacent bearers of two and three unsupported bearers, where the locations and magnitudes of the maximum load transfer show variations. Last but not least, most of the additional loads, due to unsupported bearers, are carried by adjacent bearers as recognizable in Figure 10. Other bearers in the vicinity of unsupported bearers seem to be less effective in order to support the track against additional loads (Figure 10a).



(a)



(b)

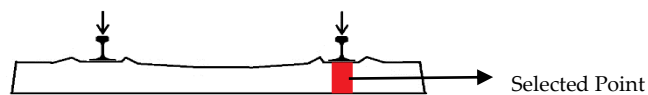
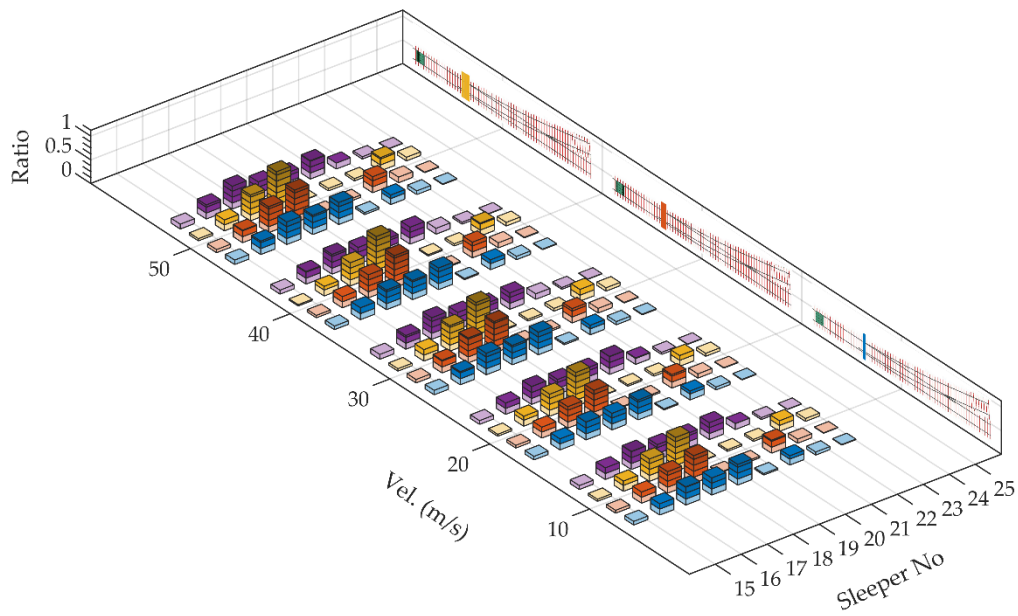


Figure 10. The distribution of rail seat force over the bearers when unsupported bearers exist at normal track section: (a) at particular time when the front wheel is on the bearer with number 10; (b) when maximum occurs at each bearer.

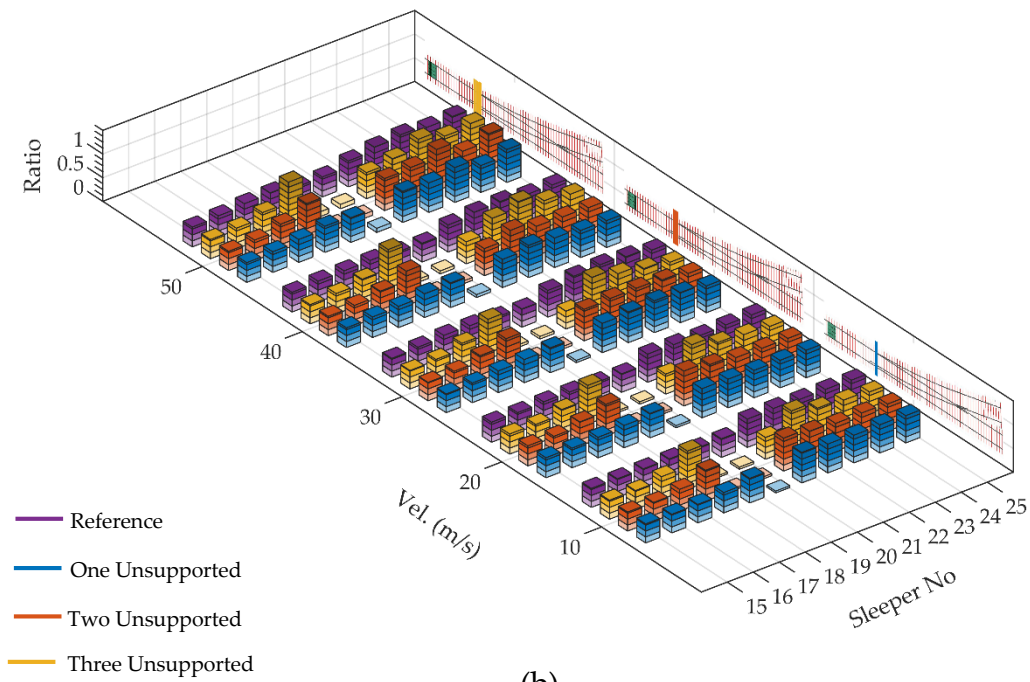
Unsupported bearers are assumed to emerge at the switch panel under switch blades in Figure 11. The lengths of the bearers are the same as the bearers at normal track section. A perceptible difference compared to the outcomes of normal section is that force transferred via fastening system is lower due to higher track stiffness introduced by switch blades. For instance, the ratio for one of the adjacent bearers is 24% less than normal track section at 50 m/s in three unsupported bearers case in Figure 11b. Furthermore, the discrepancy observed between adjacent bearers and other bearers at normal track section partially disappear here. That means loads are distributed more evenly after unsupported bearers (Figure 11a). Peculiarly, the first unsupported bearer in the facing direction (bearer no. 21) in three unsupported bearer case transfers forces significantly due to new supporting conditions created by the separation between stock rail and switch blade, where loaded rail pushes the bearer and unloaded pulls. The effect of speed seems to be unclear at this section in terms of the ratios. For example, the ratios for one of the adjacent bearers are calculated as 0.64, 0.61, 0.62, 0.59 and 0.65 from 10 m/s to 50 m/s for one unsupported bearer in Figure 11b. This outcome is also visible when relative increase considered. Relative increase is 31%, 25%, 27%, 27% and 24% under same condition.

The load distribution among the bearers under an assumption that the unsupported bearers are laid at closure panel is depicted in Figure 12. The most distinct property of the figure is that fastening systems of unsupported bearers transfer significant amount of force to the bearers, such that fastening system still carries the approximately 50% percent of the load in the reference case. This behavior has not been observed nor mentioned for fully unsupported sleepers in normal track section by current and other studies [4,5,8,9]. The ratios in adjacent bearers are between 0.44 and 0.71 based on their velocities and the number of unsupported bearers. The maximum ratio is observed at bearer number 35 when vehicle moves at 40 m/s and three bearers are unsupported. Although higher velocities seem to increase the magnitude of force transferred via fastening system in general, there is no certain pattern. For instance, the ratios from 10 m/s to 50 m/s are 0.51, 0.50, 0.55, 0.56 and 0.69 for adjacent bearer in the case of one unsupported bearer. For the same condition, the reference case has the ratios of 0.45, 0.40, 0.57, 0.46 and 0.54, respectively. The fluctuation in the ratios results from irregularities. As can be seen from the figure, the redistribution of loads is more uniform as a result of force carrying unsupported bearers.

In Figure 13, force transferred via fastening system is presented for unsupported bearers under the crossing nose. At this section, track stiffness is also relatively high due to additional rails and longer bearers, resulting in considerable force transfer between rails and unsupported bearers. As clearly present in the figure, vehicle velocity has a significant impact on force transferred via fastening system at crossing panel owing to accumulated impact forces. In terms of the effect of unsupported bearer on the force transfer, two different characteristics could be observed. At lower speed such as 10 m/s, unsupported bearers seem to have small positive effect and slightly mitigate impact forces. In this regard, the ratio for the bearer with number of 53, which is under the crossing nose, is 0.77 in the reference case whereas it is around 0.70 for unsupported scenarios. On the other hand, higher velocities cause significant force transfer. Consequently, the ratios for same bearer are at similar level (around 1.1) for one, two and three unsupported bearers and reference cases. Nonetheless, relative increase varies with respect to velocities and number of unsupported bearer since the location of impact changes also. Regarding Figure 13b, it seems that the missing ballast support has limited impact in terms of rail seat forces. This behavior becomes evident in Figure 13a, which presents the rail seat load distribution at a particular time when the front wheel is on the unsupported bearer 53.



(a)



(b)

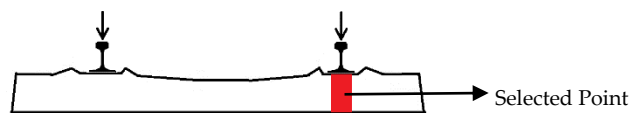
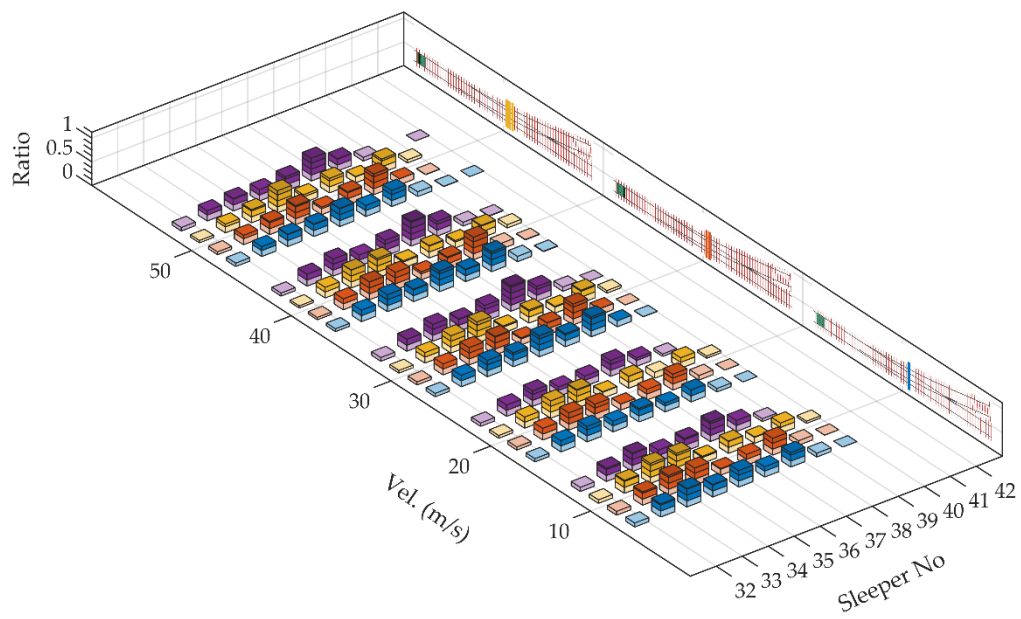
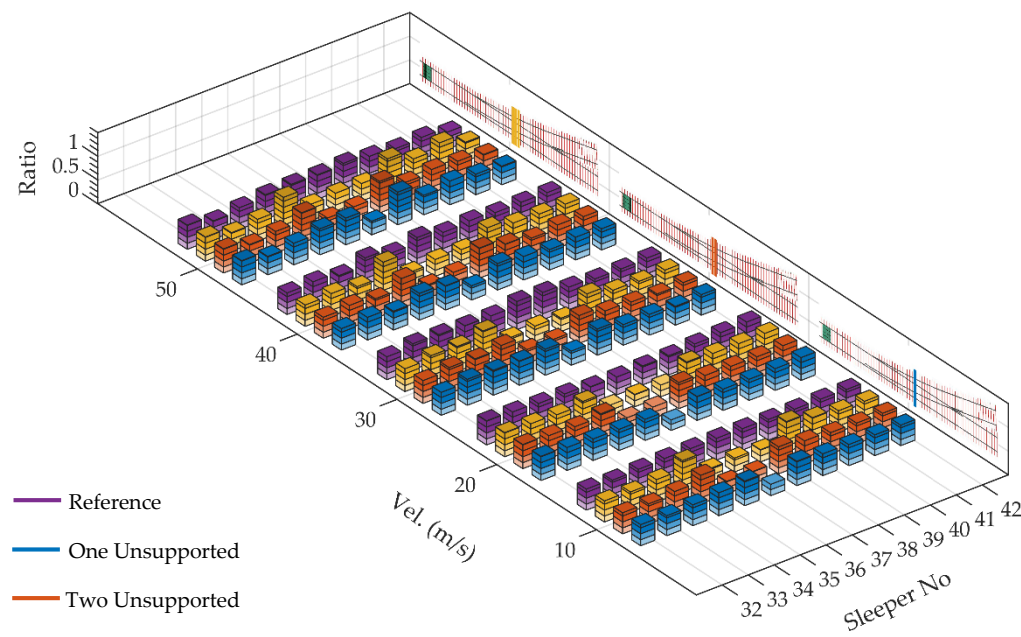


Figure 11. The distribution of rail seat force over the bearers when unsupported bearers exist under switchblades: **(a)** at a particular time when the front wheel is on the bearer with number 20; **(b)** when maximum occurs at each bearer.



(a)



(b)

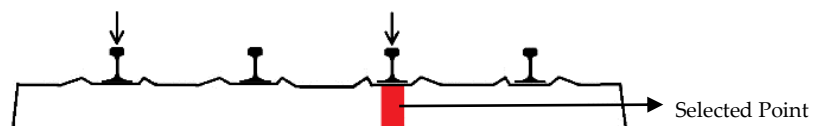
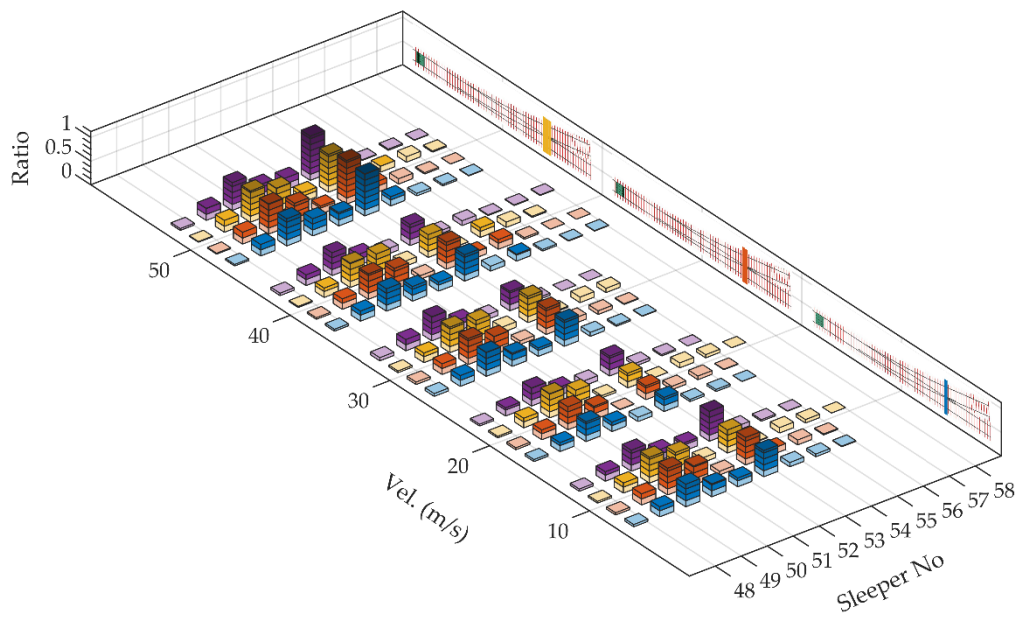
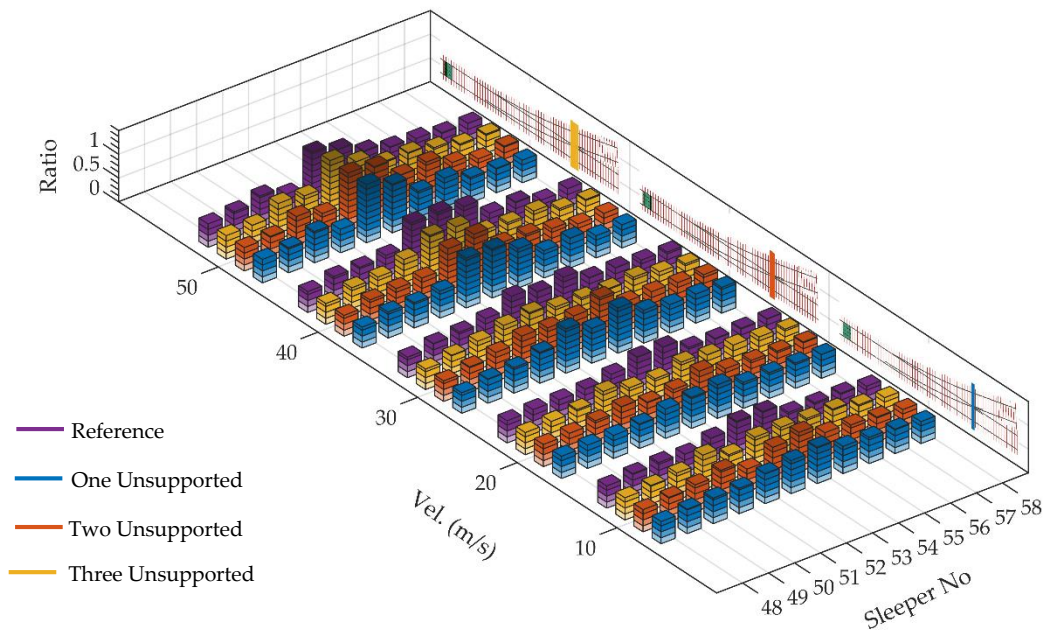


Figure 12. The distribution of rail seat force over the bearers when unsupported bearers exist at closure panel: (a) at particular time when the front wheel is on the bearer with number 37; (b) when maximum occurs at each bearer.



(a)



■ Reference
■ One Unsupported
■ Two Unsupported
■ Three Unsupported

(b)

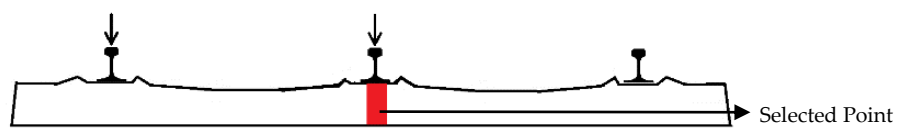


Figure 13. The distribution of rail seat force over the bearers when unsupported bearers exist under crossing nose: (a) at particular time when the front wheel is on the bearer with number 53; (b) when maximum occurs at each bearer.

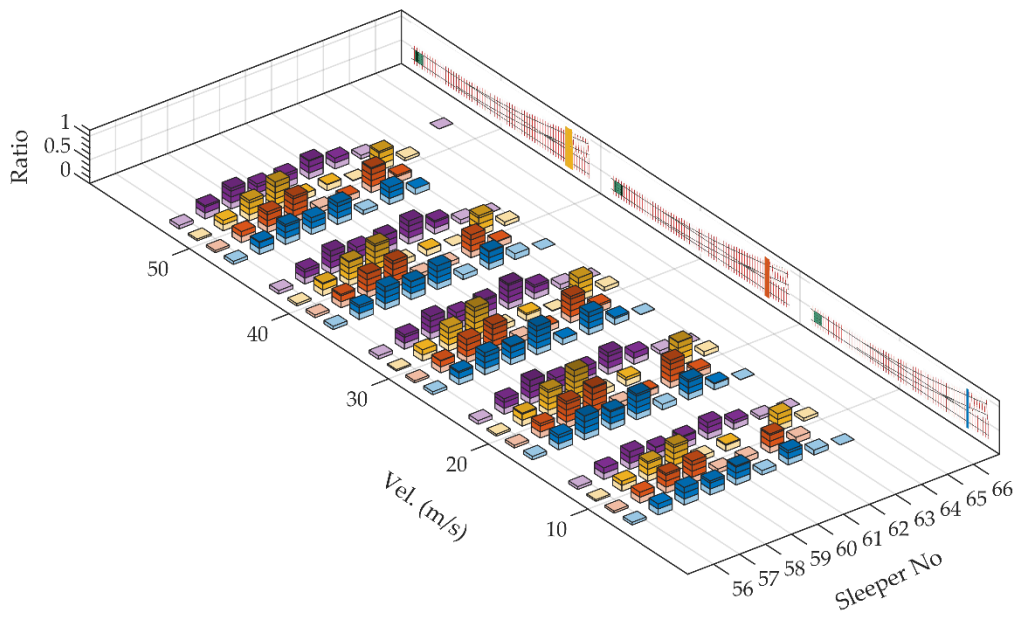
The longest unsupported bearers among the bearers following the bearers under the crossing nose carry less rail seat forces owing to the low dependency between two tracks (Figure 14). Hence, rail seat forces for adjacent bearers are considerably high in comparison to the reference case. Relative increase for adjacent bearers escalates with the number of unsupported bearers. It ranges from 19% to 80% for longest adjacent bearers, and from 10% to 135% for shortest adjacent bearers. It is also noteworthy that in the case of three unsupported bearer, one of the unsupported bearer is the shortest bearer (bearer no. 61) that is used for transition from turnout to normal track section. As can be seen from the figure, shortest unsupported bearer carries nearly no force due to independency from the diverging route when three unsupported bearer is considered.

Figure 15, plotted for the shortest bearer when it is unsupported, carries typical properties of normal track section. The unsupported bearers are clearly visible in the figure. The magnitude of the force transferred via fastening system ranges from 0.53 to 1.24. The shortest bearer provides less track support, causing a larger displacement of track and reaction forces distributed over the bearers. It also should be noted that the longest bearer is also in the vicinity of shortest bearer, having higher track stiffness. Consequently, load distributions are more uneven at this section, causing that shortest bearer carries relatively higher forces, when maximum rail seat forces are considered. In all cases, the latter adjacent bearers carry much of the loads compared to other adjacent bearer, which is different from the case of unsupported bearers at normal track section. Relative increase range from 22% to 198% associated with vehicle velocity and the number of unsupported bearers. When considering the results for a particular time (Figure 15a), this behavior is vice versa. Former adjacent bearer is subjected to higher forces as the rear wheel also affects it.

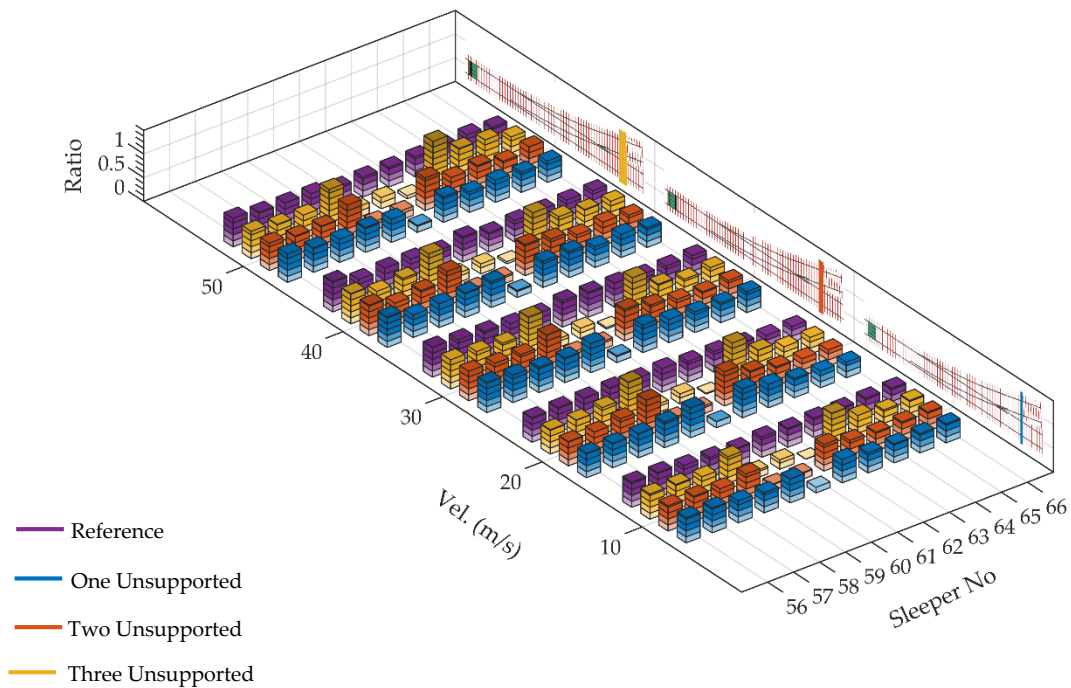
3.4. Negative Bending Moment Distributions of Selected Points

Bending moment distributions along a turnout show quite complex behavior. In general, maximum positive bending moments occur at rail seats in contrast to maximum negative bending moments that could exist at any position along a bearer [12]. Therefore, it seems more suitable to select a specific position on the bearer to investigate negative bending moment behaviors. Indeed, it is a challenging task due to varying bearer lengths and additional rails such as switchblades. It is obvious that other ends of the bearers will have different coordinates due to varying lengths, regarding one-sided alignment of the bearers. A common approach is to select midpoints of bearers and rail seats while investigating the response of the system for normal track. The same idea is followed here with a small adaptation referring to above-mentioned challenge. Here, the element in the middle of two loaded rails is selected instead of mid-point of a bearer.

Maximum negative bending moments of middle points of the bearers at normal track section are illustrated in Figure 16. It seems that the figure reveals the common characteristic behavior of unsupported bearers at normal track section. Unsupported bearers carry no significant force that results in no bending moments in contrast to supported adjacent bearers. Furthermore, the more unsupported track section expands, the higher negative bending moments occur over fully supported bearers. Maximum negative bending moments of supported bearers could reach 8.8 kNm, while three bearers are unsupported at 50 m/s. The changes in the velocity mostly cause higher bending moments as also found in [3]; however, the effect of velocity owing to unsupported bearers is unclear in comparison with the reference case. For instance, relative increase for one of the adjacent bearers are 33%, 35%, 27%, 34% and 45% at 10 m/s, 20 m/s, 30 m/s, 40 m/s and 50 m/s, respectively, in the case of one supported bearer.



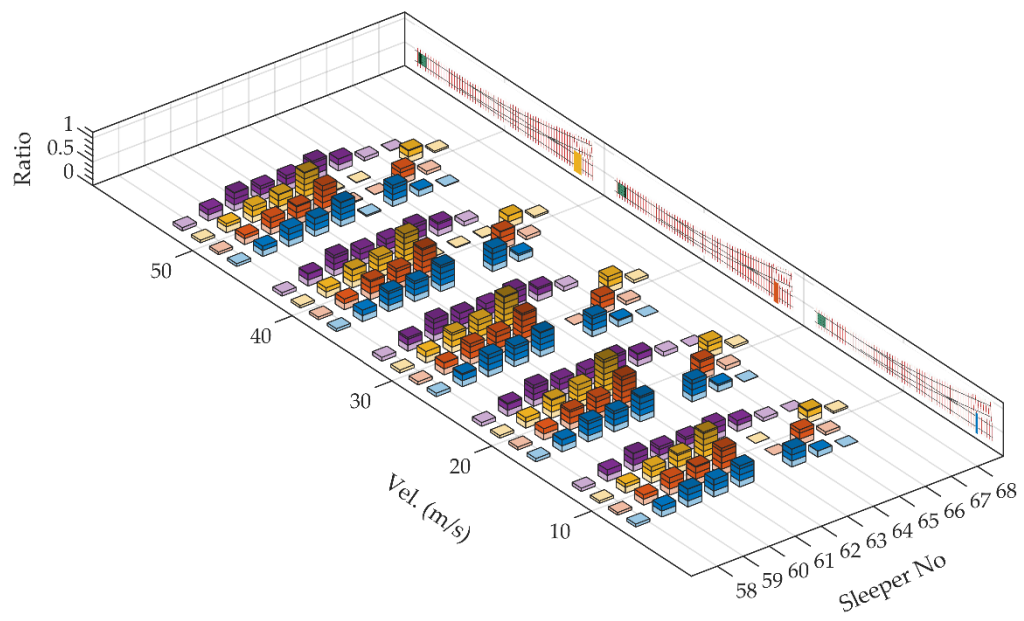
(a)



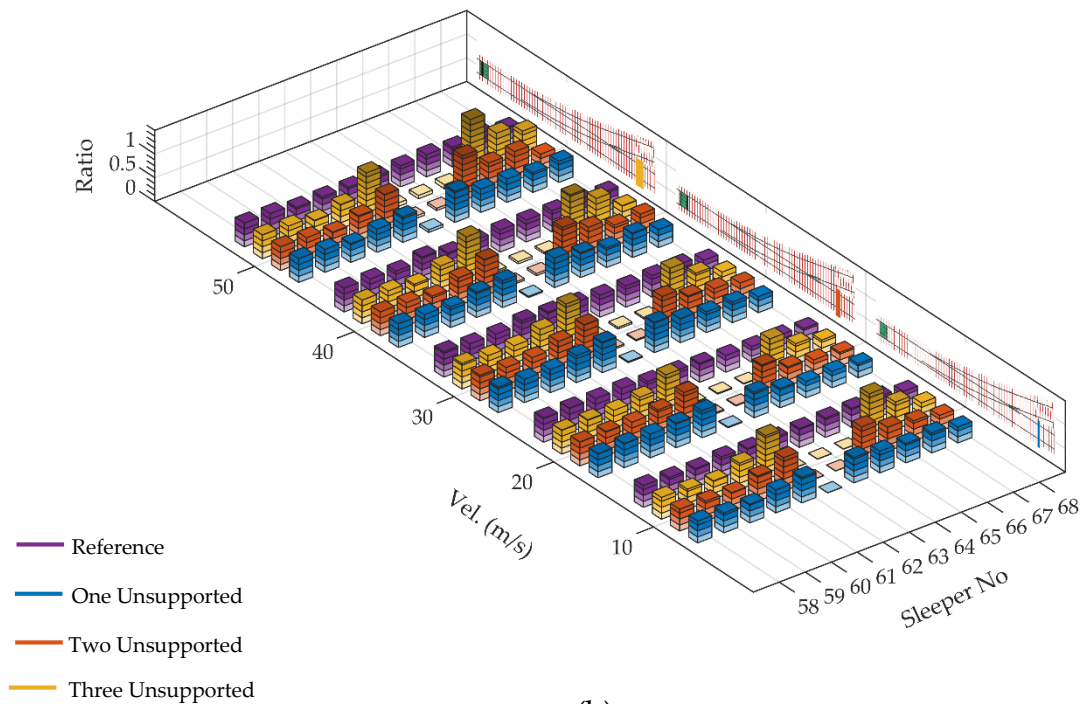
(b)



Figure 14. The distribution of rail seat force over the bearers when the longest bearer is unsupported: (a) at particular time when the front wheel is on the bearer with number 61; (b) when maximum occurs at each bearer.



(a)



(b)

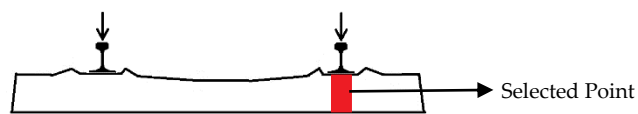


Figure 15. The distribution of rail seat force over the bearers when the shortest bearer is unsupported: (a) at particular time when the front wheel is on the bearer with number 62; (b) when maximum occurs at each bearer.

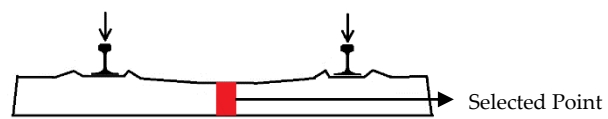
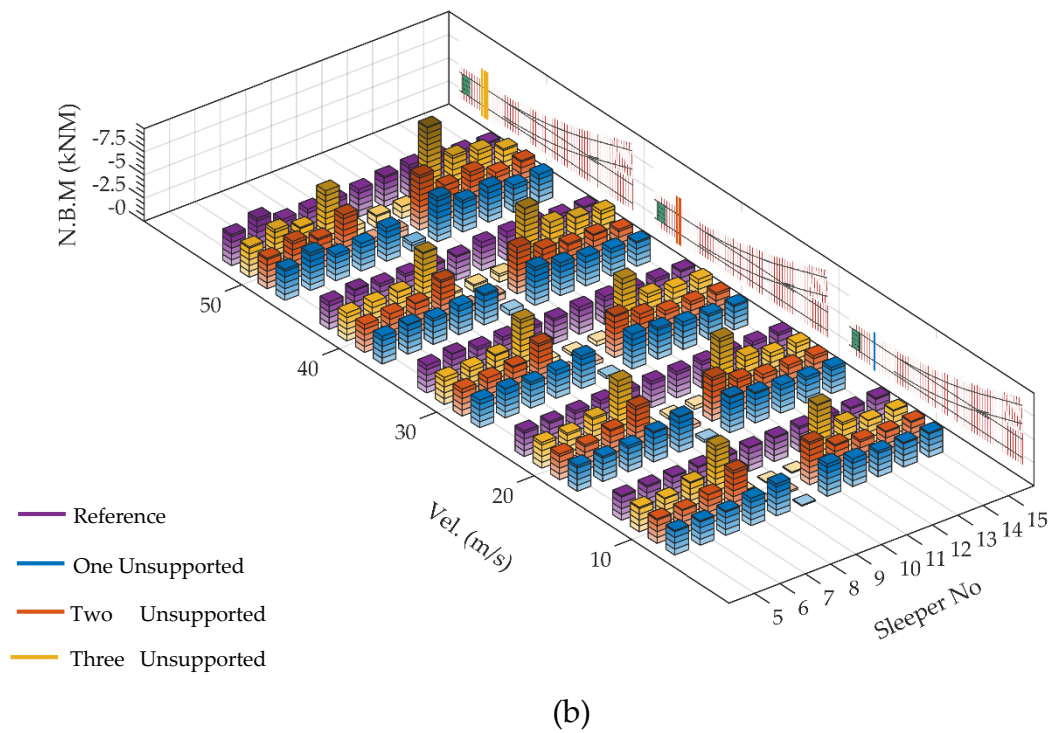
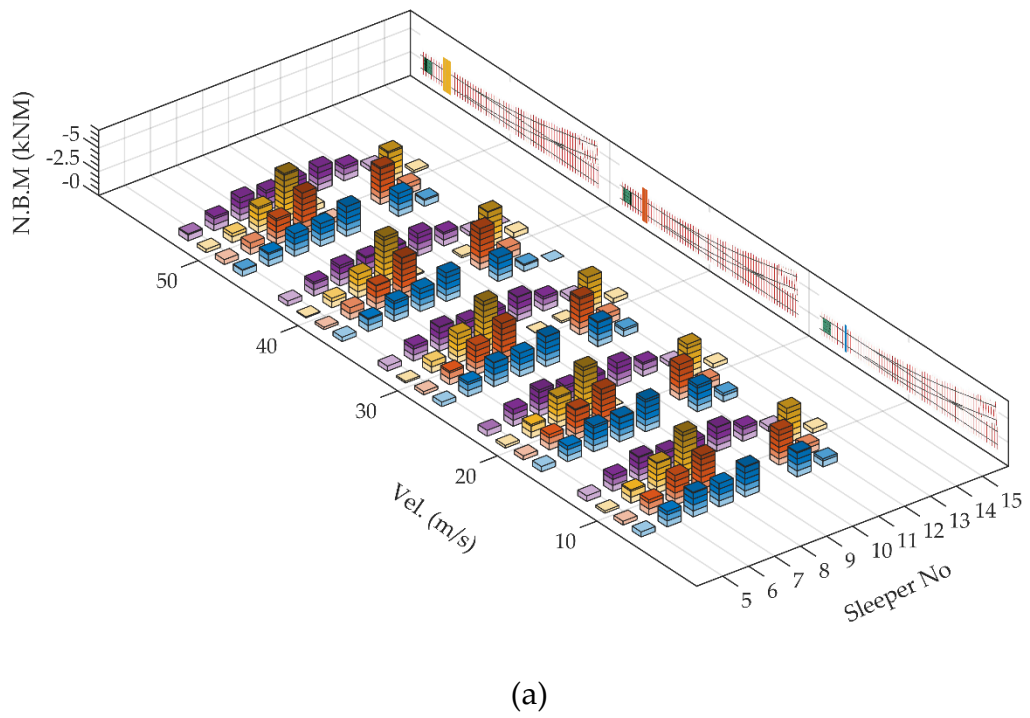


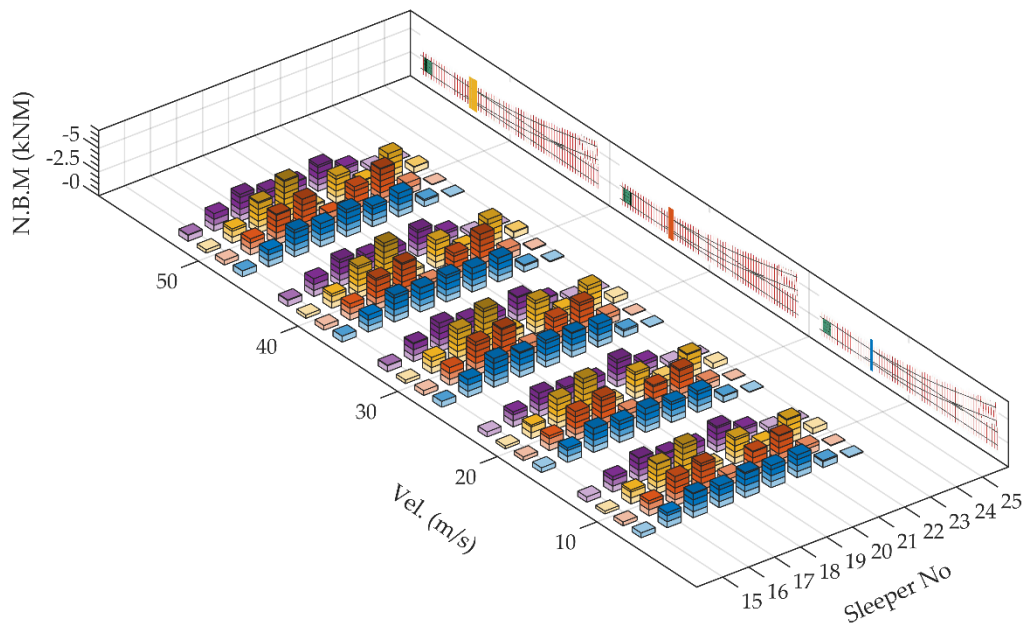
Figure 16. The distribution of negative bending moments over the bearers when unsupported bearers exist at normal track section: (a) at particular time when the front wheel is on the bearer with number 10; (b) when maximum occurs at each bearer.

A depiction of the results for the unsupported bearers laid under switchblades is given in Figure 17. What stands out in the figure is that the distributions of maximum negative moments for unsupported bearers show no distinct deviation from the reference case. The reason why unsupported bearers are subjected to a negative bending moment is that switch blades, specifically opened switch blade, act as a support that cause negative bending moments [12]. The maximum negative bending moments range from 3.1 kNm to 5.8 kNm for bearers under switch blades. Despite one different case when three bearers are unsupported, maximum negative bending moment is correlated to the number of unsupported bearers, in contrast to different speeds, in terms of bending moments of unsupported bearers. For instance, the magnitudes of bending moments of same bearer are 2.5, 2.8 and 3.1 kNm for one, two and three unsupported cases.

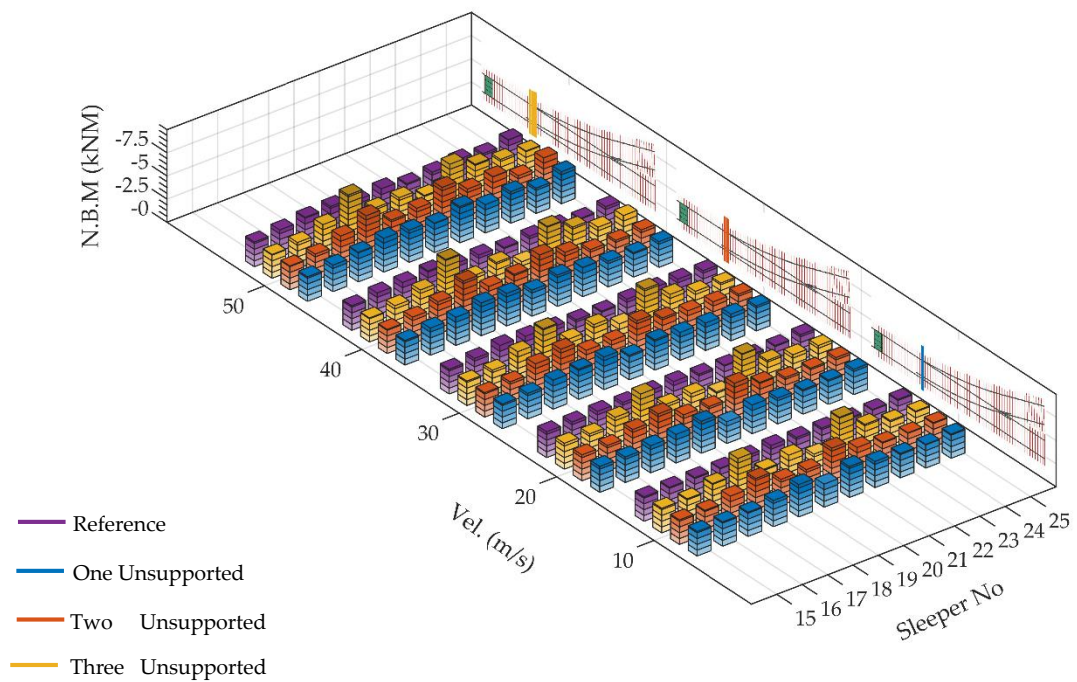
Similar to switch panel, unsupported bearers also bear maximum negative bending moments when they are laid at closure panel, shown in Figure 18. It is clear that unsupported bearers amplify negative bending moments at closure panel. More interestingly, they are subjected to considerable negative bending moments and the contribution of vehicle speed to negative bending moments is imperative compared to other sections; whereas force transferred via fastening system is the lowest at this section with no significant effect of vehicle speed, as indicated previously. The highest magnitudes of maximum negative bending moment occur at bearer 37 in most cases. The exception is the case when three unsupported bearer exist and vehicle velocity is 50m /s. That time maximum negative bending moment shifts to the bearer with number 38, which is the worst case with a magnitude of 6.5 kNm that is 58% higher than reference case. What is more interesting is that the adjacent bearers of unsupported bearers are exposed to lower bending moments than unsupported bearers (Figure 18b), which is mostly vice versa in other cases.

Figure 19 compares the outcomes of the simulations in terms of maximum negative bending moments of the bearers at crossing panel when the unsupported bearers are assumed to occur under the crossing nose. It is apparent from the figure that there is a difference between lower and higher speeds. At lower speeds such as 10 m/s, the impact forces are relatively ineffective and behavior of bearers is akin to normal track sections where the unsupported bearers are subjected to relatively no bending moments. Therefore, adjacent bearers are affected more from maximum negative bending moments. It should also be emphasized that an idle closure rail between two rails, producing negative bending moments, disappears at this section. On the other hand, the magnitude of impact forces escalates with higher velocities, which result in higher negative bending moments. Nevertheless, they are still lower than the reference case. In the worst case, maximum negative moment is 30% below the reference case.

As there is no additional rail between two loaded rails, maximum negative bending moments at the selected point of longest bearer show similar behavior to normal similar (Figure 20). Unsupported bearers carry insignificant loads. The striking difference is that negative bending moments for longest adjacent bearers of unsupported bearers are lower than the shortest adjacent bearers. For instance, the magnitudes of maximum negative bending moments are 2.7/3.8, 3.4/4.3 and 4.5/6.04 kNm for longest/shortest adjacent bearers in one, two and three unsupported bearer cases, respectively. The reason could be explained by two factors. As previously mentioned, the load distribution is asymmetrical in this case, resulting in higher forces on the shortest bearers. Moreover, the actual maximum negative bending moments could occur on diverging route due to support conditions whereas the maximum negative bending moment depicted above is valid for bearer section located in the middle of two tracks. Although the results in Figure 20a seem to contradict with the outcome in previous sentences, it should be stressed that the results in Figure 20a is plotted when the front wheel is on the top of an unsupported bearer. As a consequence, the rear wheel also has a share in the negative bending moments of longest adjacent bearer at the particular time.



(a)



(b)

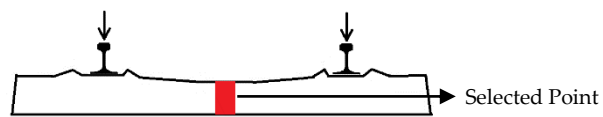


Figure 17. The distribution of negative bending moments over the bearers when unsupported bearers exist under switchblades: (a) at particular time when the front wheel is on the bearer with number 20; (b) when maximum occurs at each bearer.

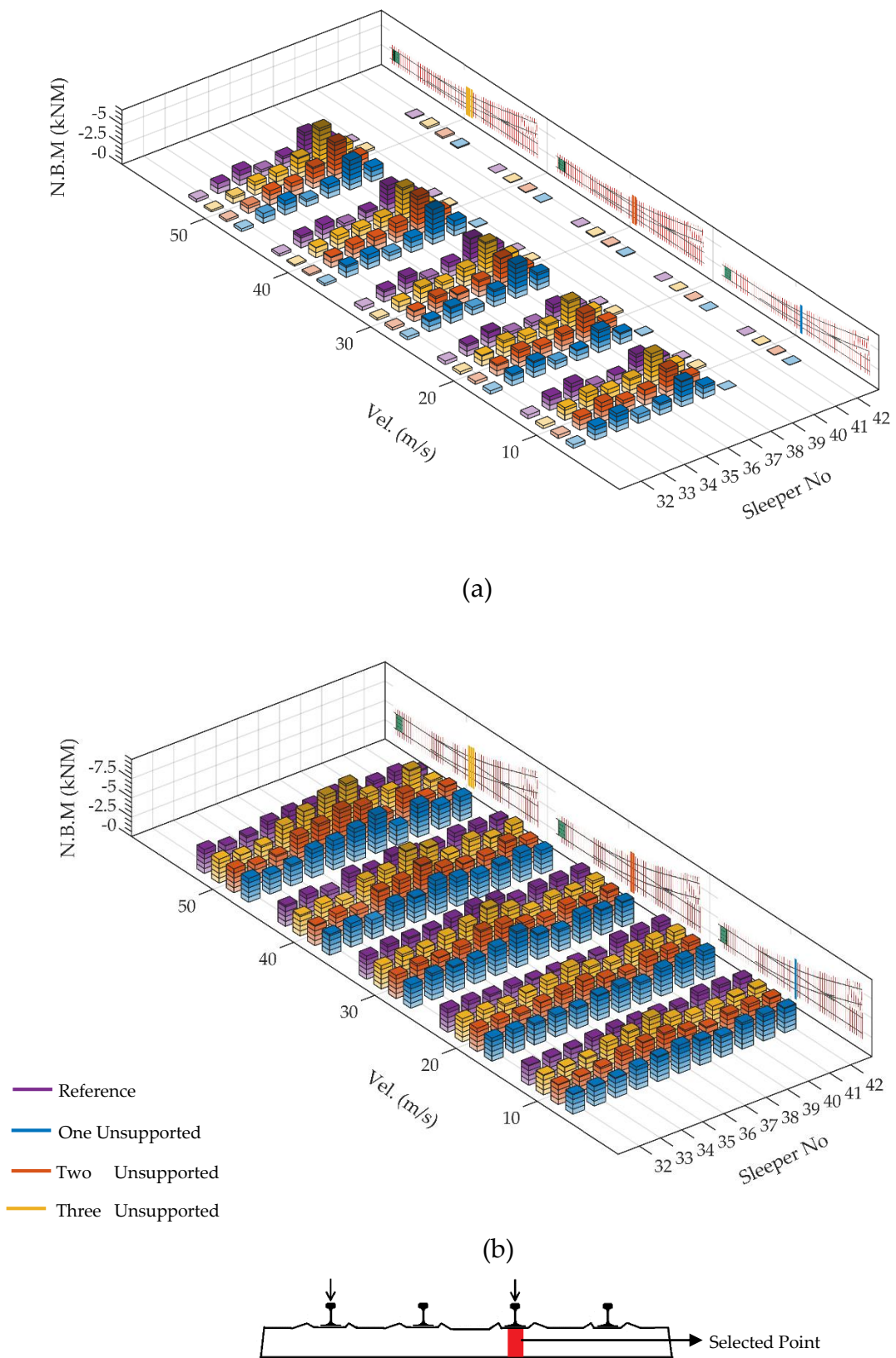
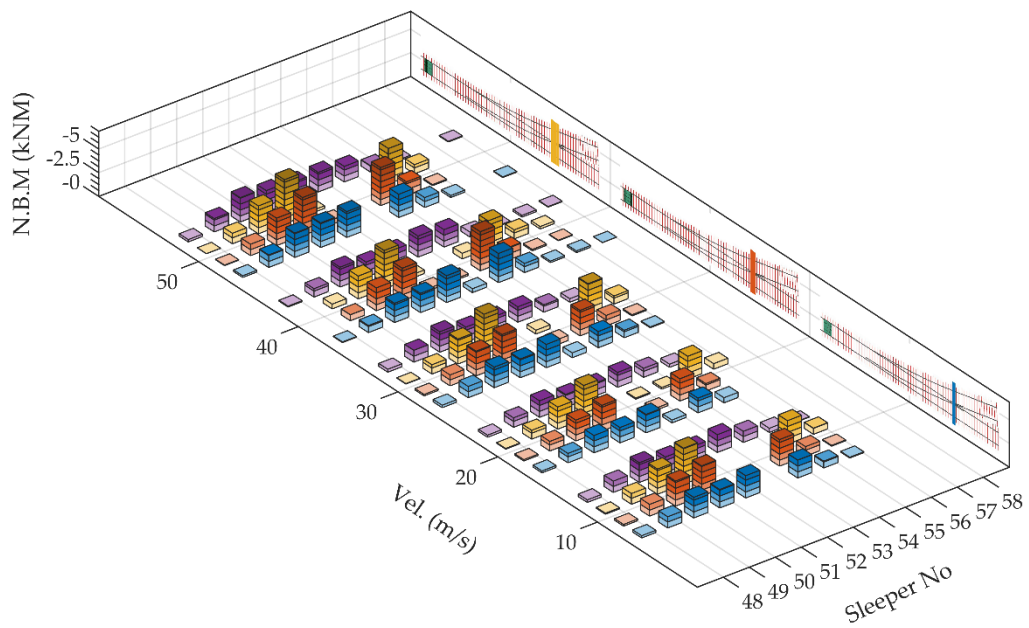
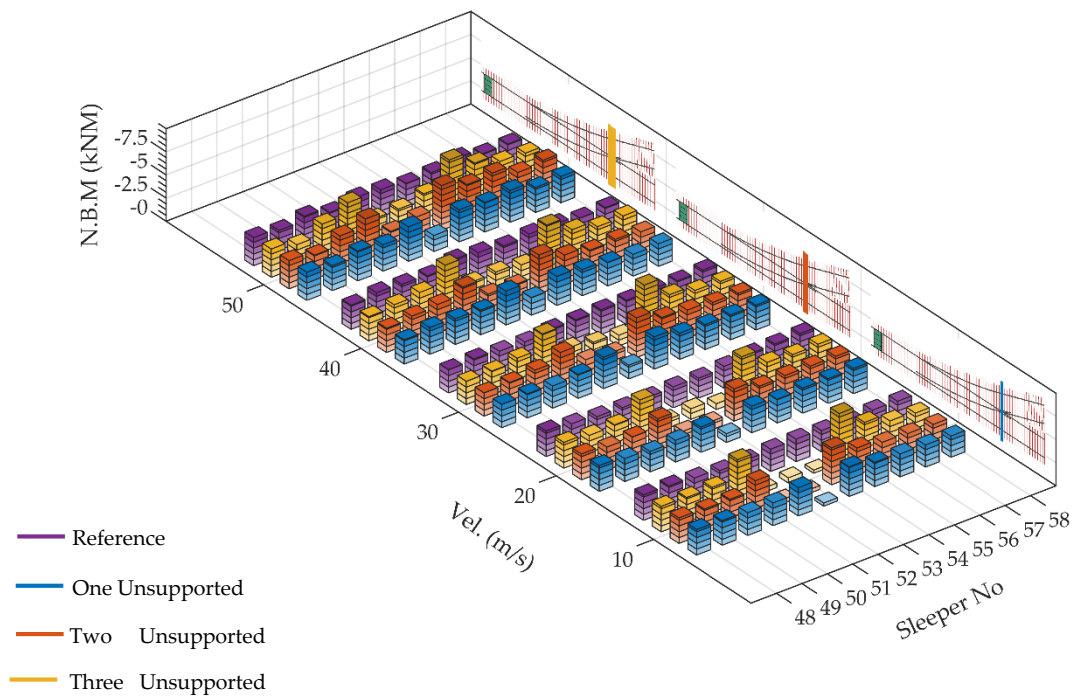


Figure 18. The distribution of negative bending moments over the bearers when unsupported bearers exist at closure panel: (a) at particular time when the front wheel is on the bearer with number 37; (b) when maximum occurs at each bearer.



(a)



(b)

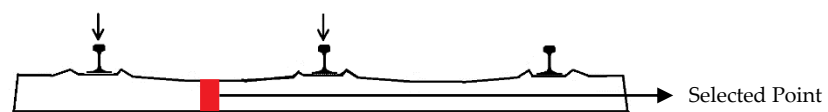
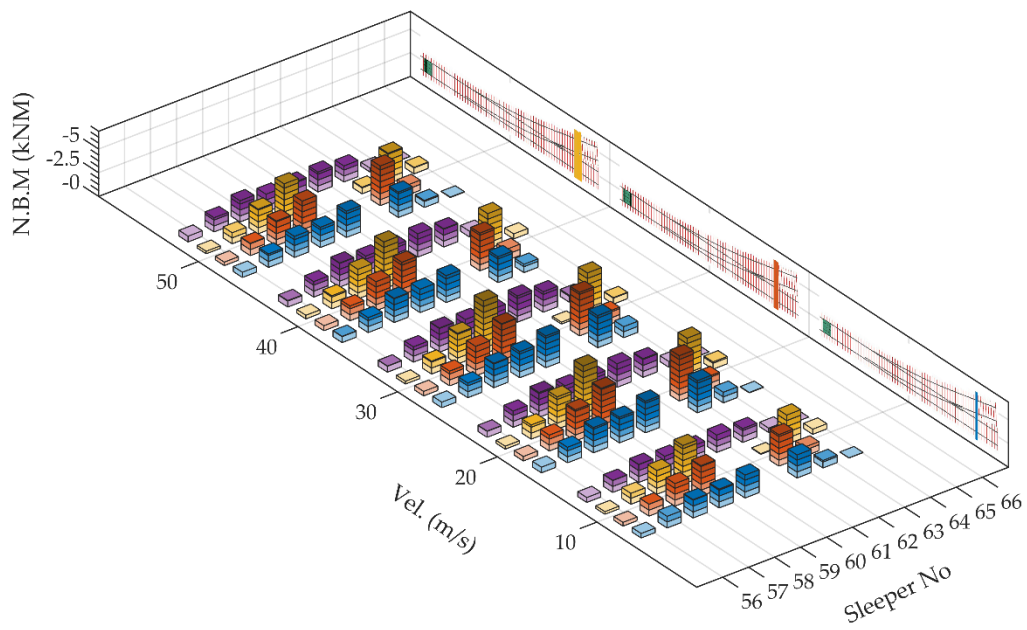
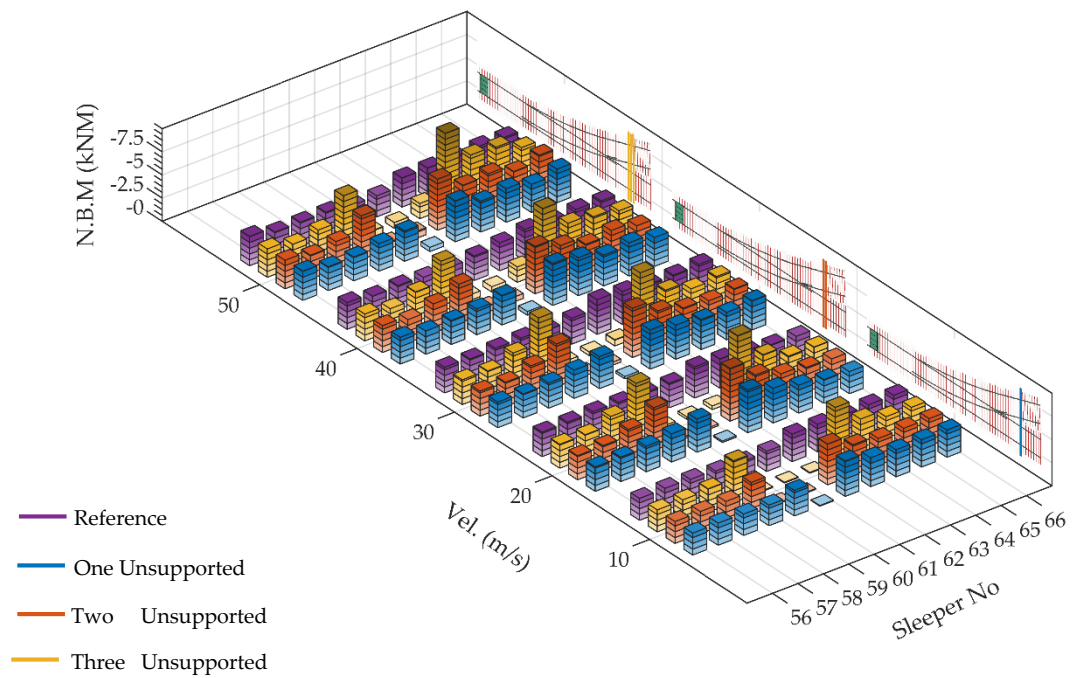


Figure 19. The distribution of negative bending moments over the bearers when unsupported bearers exist under crossing nose: (a) at particular time when the front wheel is on the bearer with number 53; (b) when maximum occurs at each bearer.



(a)



(b)

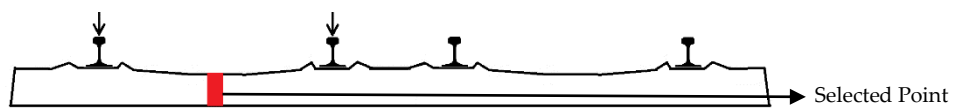


Figure 20. The distribution of negative bending moments over the bearers when the longest bearer is unsupported: (a) at particular time when the front wheel is on the bearer with number 61; (b) when maximum occurs at each bearer.

The contribution of shortest bearers becomes evident in Figure 21, in which it is assumed that shortest bearers are unsupported and the results for that case are plotted. The figure shows similar trend with normal track section where adjacent bearers of the unsupported bearers are subjected to higher negative bending moments. Furthermore, it is clear that the number of unsupported bearers affect the maximum negative bending moments. Differently, one could remember that forces transferred via fastening system are highest at the shortest bearer. Inherently, negative bending moments are expected to be highest at this section due to higher deflections. The magnitudes of negative bending moments differ from 3.8 to 9.3 kNm for adjacent bearers. Likewise, relative increase varies between 23% and 184%. Another different property of the figure is that the transition between longest bearer and shortest bearer results in significant negative bending moment difference in all cases, which is between 1.3 and 4.7 kNm based on the case and the velocity. Last but not least, a common approach in the railway applications is that the middle section of the bearers is left loose to decrease negative bending moments. This application seems to be crucial for shortest bearers regarding the results in the figure. Extra attention should be given while maintaining the shortest bearer due to amplification factor of unsupported bearer at this section.

3.5. Positive Bending Moment Distributions of Selected Points

In the previous research, it is found that the maximum positive bending moments appear at rail seats of turnout bearers [12], which is similar to normal tracks [23–27]. The same idea is applied here while assessing the relation between unsupported bearers and positive bending moment distribution along a turnout.

As reflected in Figure 22, the distribution of maximum positive bending moments of bearers at normal track section shows similarities with the distribution of force transferred via fastening system and maximum negative bending moments in previous section. Unsupported bearers have no significant positive bending moments and an increased number of unsupported bearers introduce higher bending moments on adjacent bearers. Similarly, the effect of different velocity is unclear. For instance, two unsupported bearers cause maximum positive bending moments of 8.5 kNm, 8.6 kNm, 8.5 kNm, 8.3 kNm and 8.7 kNm over one adjacent bearer at 10 m/s, 20 m/s, 30 m/s, 40 m/s and 50 m/s, respectively. Under the same condition, maximum positive bending moments over the other adjacent bearer are 8.4 kNm, 8.5 kNm, 8.3 kNm, 9.1 kNm and 10.6 kNm. Furthermore, the plot in a particular time also follows the similar pattern. The distribution becomes more uneven with unsupported bearers and transition the from adjacent bearer to the next fully supported bearer is sharp.

A distribution of maximum positive bending moments owing to unsupported bearers is depicted in Figure 23 for switch panel bearers. Similar properties observed in normal track section are also valid for the bearers at switch panel. Apart from that, a small discrepancy could be observed in the case of three unsupported bearers, where one of the unsupported bearers, first one in moving direction, has positive bending moments due to additional rail that acts like a support. In numerical model, this bearer is the point before which the switch blades and stock rails just start to split. In general, the correlation remains between the force transferred via the fastening system and the maximum positive bending moments at this section. In all cases, the maximum positive bending moment take place at former adjacent bearer of unsupported bearers. Among them, highest maximum positive bending moment, 11.5 kNm, emerges at 50 m/s when three bearers are unsupported and lowest positive bending moment is 5.2 kNm at 10 m/s with two unsupported bearer. Considering the positive bending moment distributions in particular time, it is evident that the distribution looks similar to normal track section. The only difference is the positive bending moments seems to be distributed more evenly due to higher track stiffness.

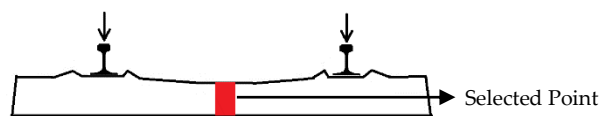
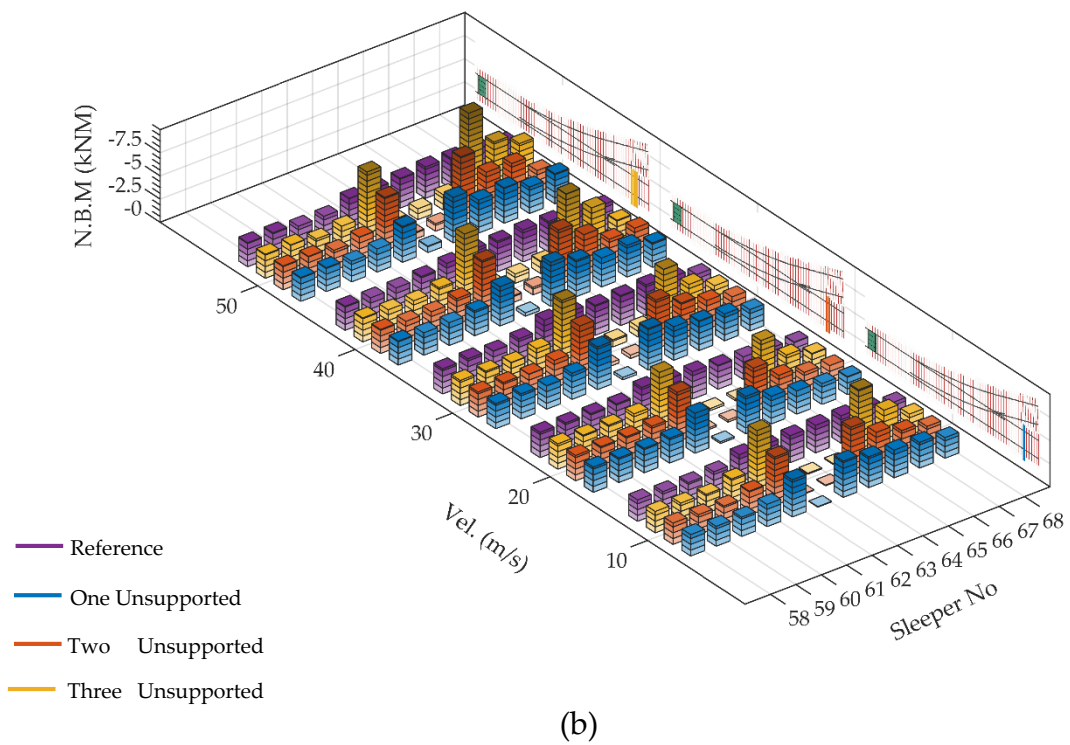
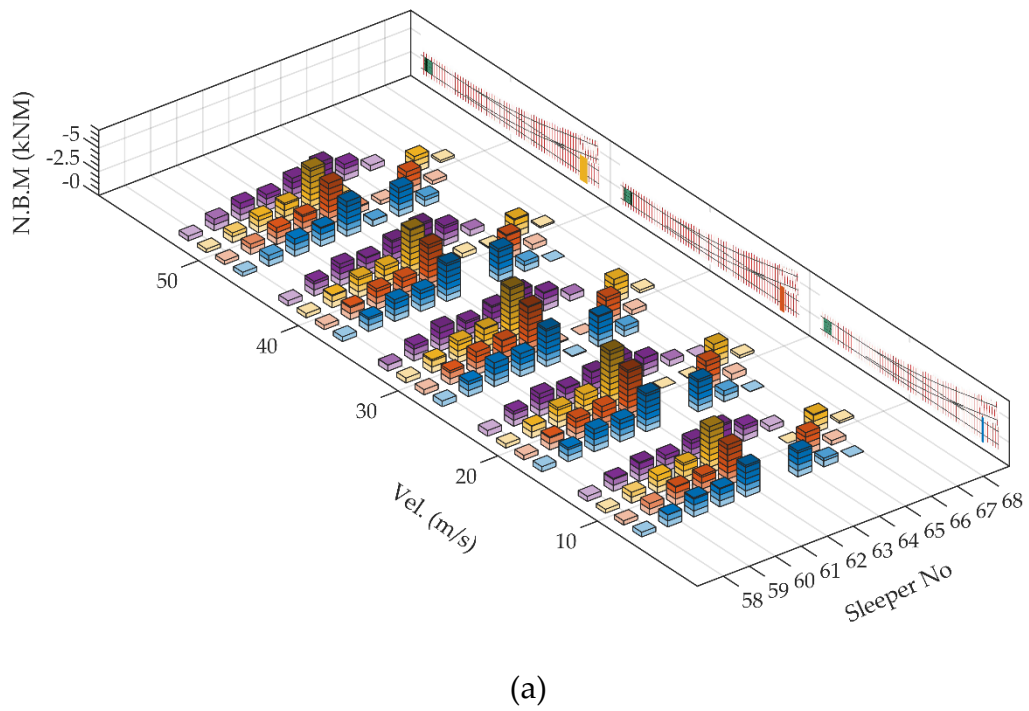


Figure 21. The distribution of negative bending moments over the bearers when the shortest bearer is unsupported: (a) at particular time when the front wheel is on the bearer with number 62; (b) when maximum occurs at each bearer.

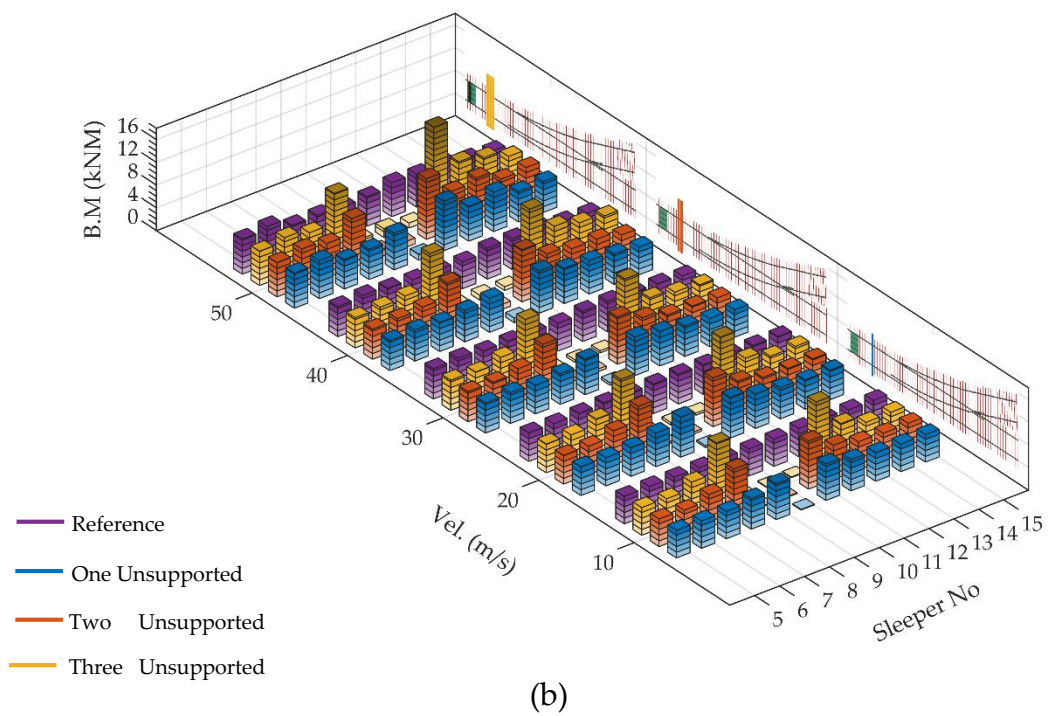
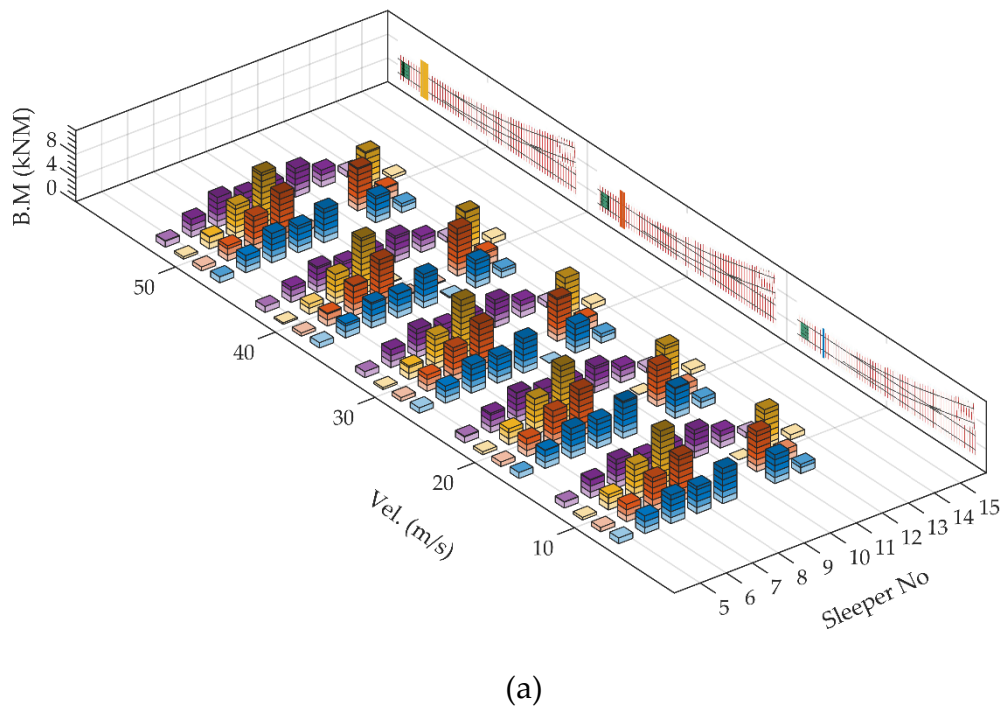


Figure 22. The distribution of positive bending moments over the bearers when unsupported bearers exist at normal track section: (a) at particular time when the front wheel is on the bearer with number 10; (b) when maximum occurs at each bearer.

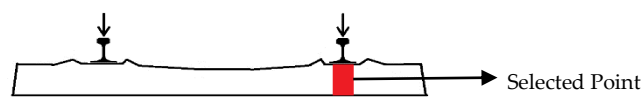
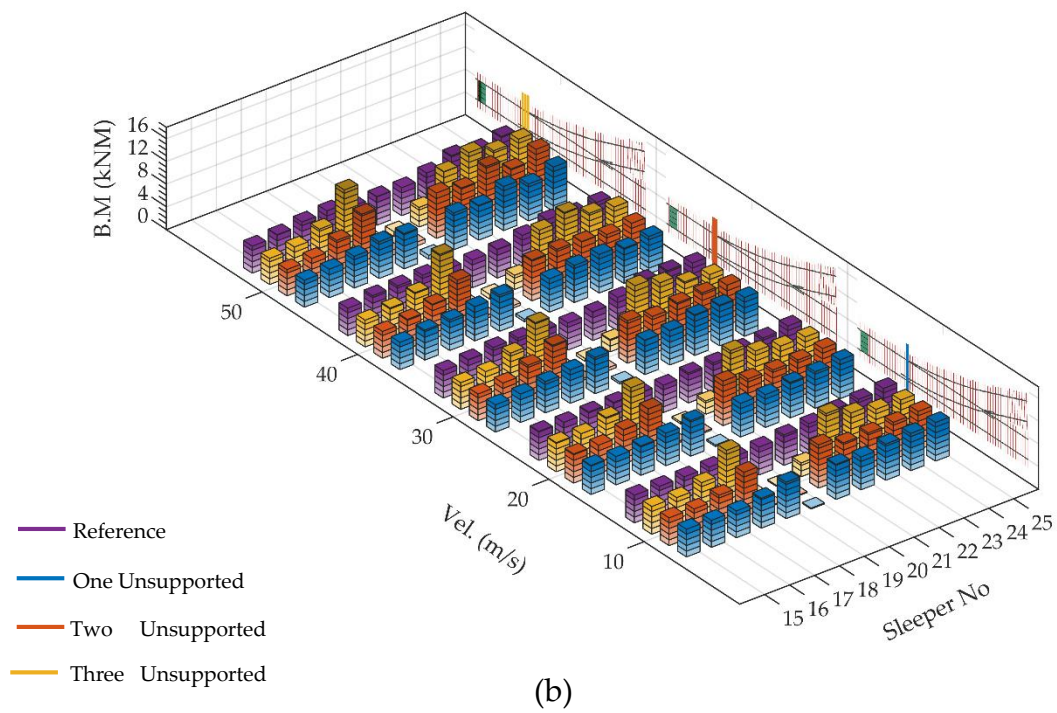
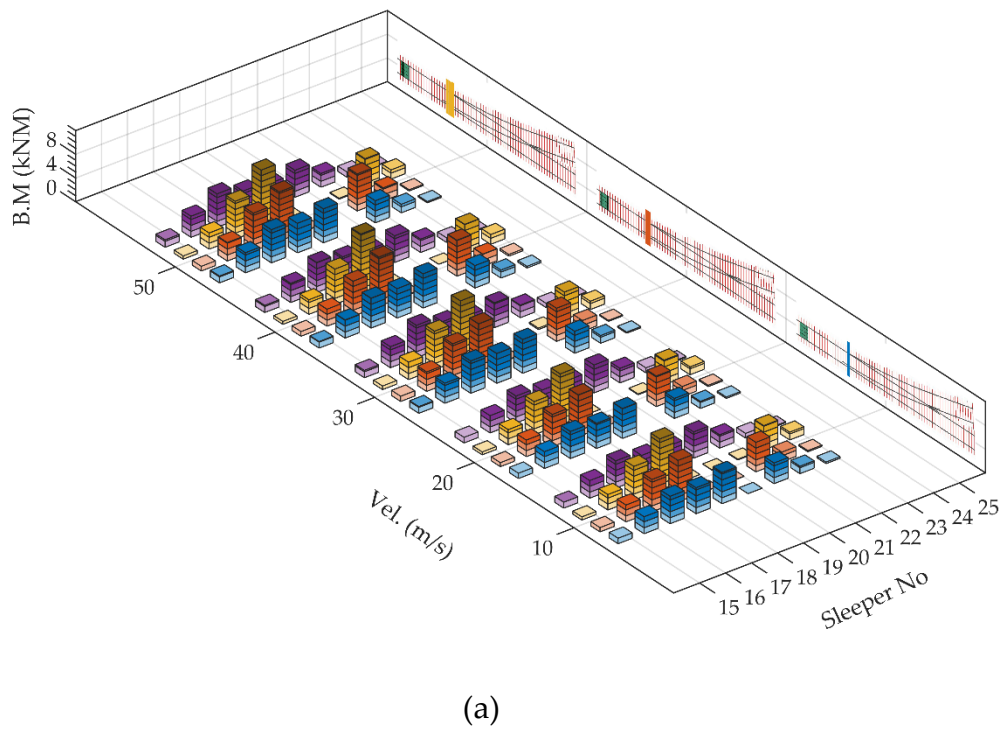


Figure 23. The distribution of positive bending moments over the bearers when unsupported bearers exist under switchblades: (a) at particular time when the front wheel is on the bearer with number 20; (b) when maximum occurs at each bearer.

As can be seen from Figure 24, reflecting the effect of unsupported bearers at closure panel, the unsupported bearers are also exposed to important positive bending moments. It could be said that the results for all three cases is indistinct in terms of maximum positive bending moments at this section, despite a barely perceptible difference for adjacent bearers having slightly higher positive bending moments. According to [12], highest bending moments occur at closure panel under static loads or at lower speeds, when the impact forces are ineffective at crossing nose. Relative bending moments range from -1.3 kNm to 1 kNm for unsupported bearers at different speeds. Likewise, relative bending moments for adjacent bearers vary from -0.72 kNm to 2.01 kNm, associated with vehicle speed and number of unsupported bearers. Here, negative sign indicates that bending moments in reference case could be higher, regarding the previously made definition of 'relative'. Apart from that, the plot of bending moments in particular time shows that the bending moments reach maximum when the wheel is on the top of unsupported bearer. What is more, the bending moment value for that bearer exceeds the other values where rear wheel contribution takes place. Hence, it is expected that unsupported bearers underneath the closure panel is likely to be damaged quickly.

In Figure 25, maximum positive bending moments as a result of unsupported bearers under crossing nose are presented. Two distinct properties are striking. First, unsupported bearers at lower speeds have relatively small bending moments due to lower contact forces, which is similar to negative bending moments. As aforementioned, adjacent bearers have relatively higher load distribution due to insignificant impact loads at lower speeds. The combination of this uneven load distribution and length of the bearers result in higher bending moments. Hence, adjacent bearers are affected from relatively higher bending moments regarding the reference case. Adjacent bearer have up to 26%, 51% and 78% increase ratio for one, two and three unsupported bearer. On the other hand, higher speeds induce significant impact forces. Those impact forces result in higher bending moments at unsupported bearer or bearers after crossing nose with reference to different velocities. As a result, the gap between adjacent bearer and unsupported bearer closes. Interestingly, the unsupported bearers have positive effect to mitigate impact forces at crossing nose. The reduction in positive bending moments could be up to 56% at 10 m/s and 21% at 50 m/s. This behavior seems to be different for concrete bearers, which will be mentioned in later in this paper.

Maximum positive bending moments are given in Figure 26, for unsupported longest bearer and its neighbor bearers. Even though the track is relatively separated from diverging track, unsupported bearers are still subjected to positive bending moments that are lower in the magnitude and more, adjacent bearers have relatively higher bending moments. Magnitudes for adjacent bearers vary from 4.8 to 11.7 kNm with respect to different velocities. For unsupported bearers, it is between 3.2 and 6.2 kNm. As clearly seen in the figure, one of the unsupported bearers (shortest bearer) carries no positive bending moments, which is due to independency from diverging route. Another perceptible difference is that longest adjacent bearers are subjected to more bending moments in comparison to shortest adjacent bearer as a result higher track stiffness.

As demonstrated in Figure 27, shortest bearers have lower maximum positive bending moments owing to their shorter lengths. The distribution characteristic is similar to normal bearers. The unsupported bearers have almost no bending moments and the number of unsupported bearers significantly affects the bending moments of adjacent bearers. The maximum positive bending moment is observed with a magnitude of 12.3 kNm at 50 m/s in the case of three unsupported bearers. Similarly, the effect of vehicle velocity is also unclear at this section. For instance, the magnitudes of maximum positive bending moments are 9.5, 7.3, 8.5, 10 and 12.3 kNm from 10 m/s to 50 m/s, respectively, for one of the adjacent sleepers in three unsupported case.

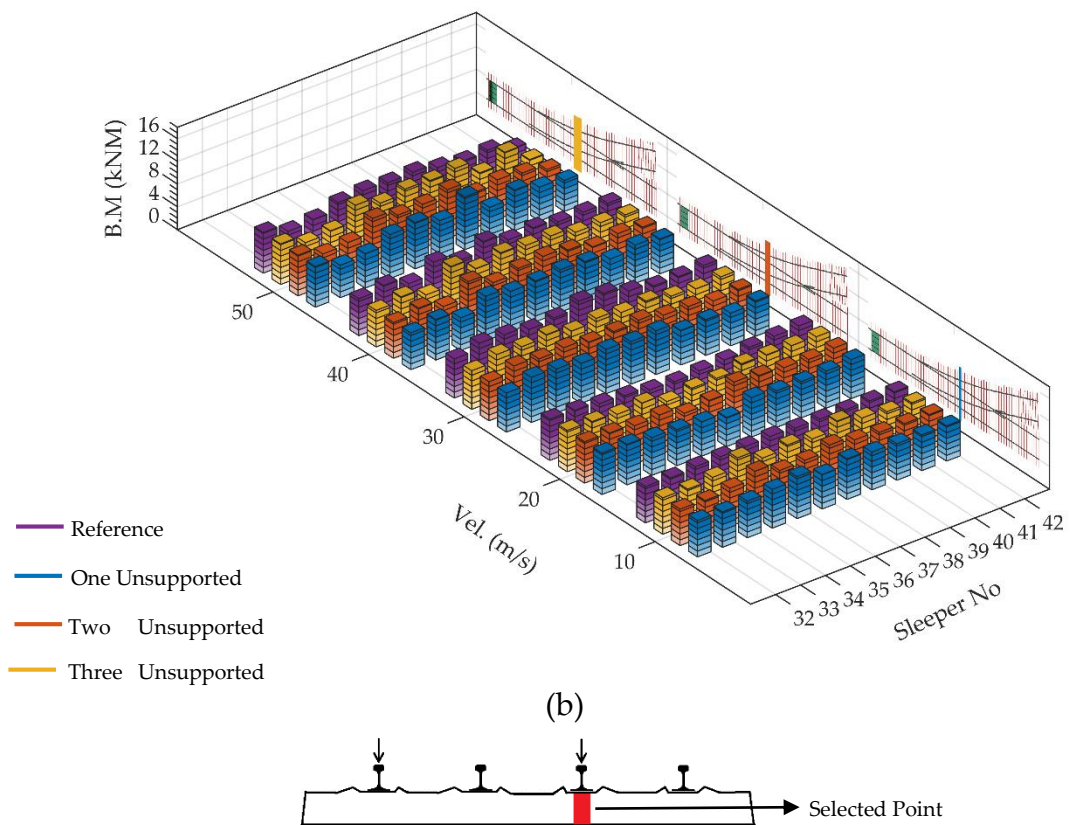
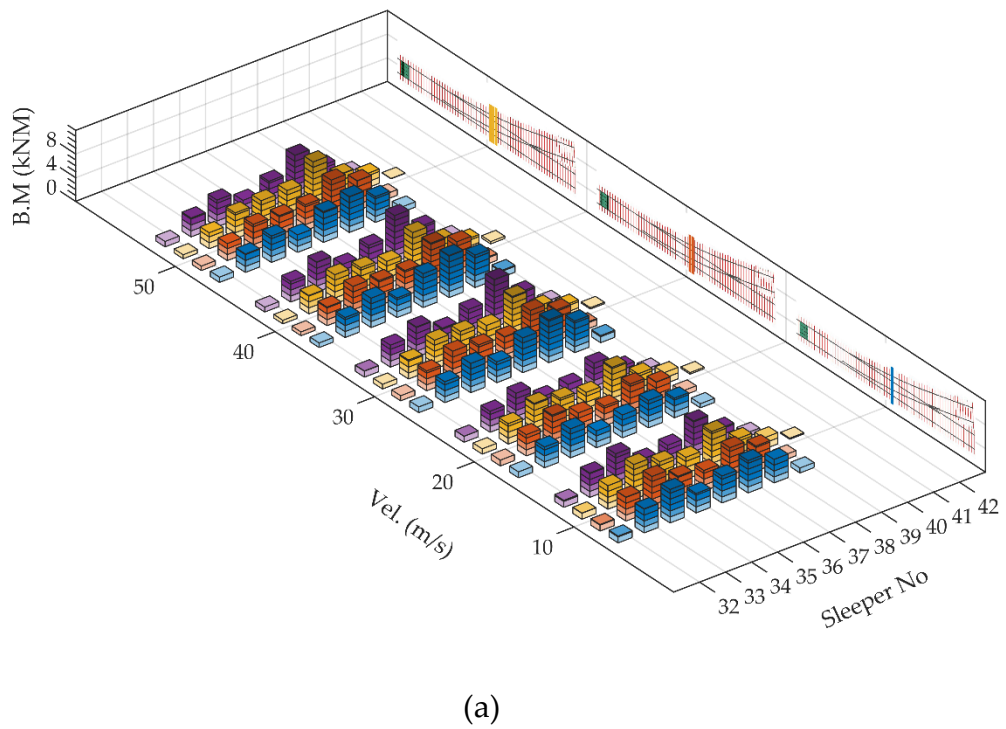
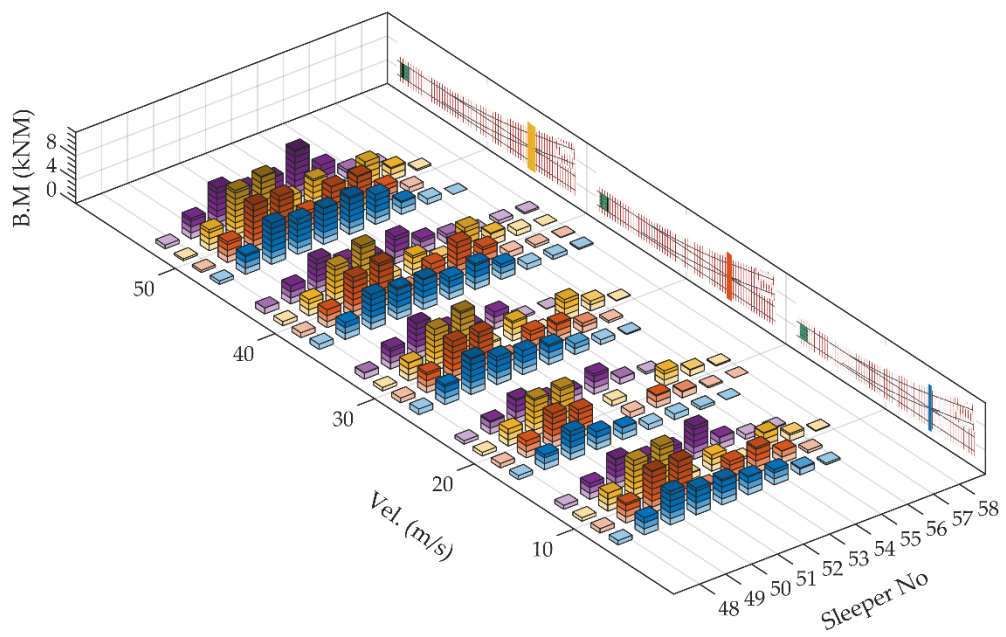
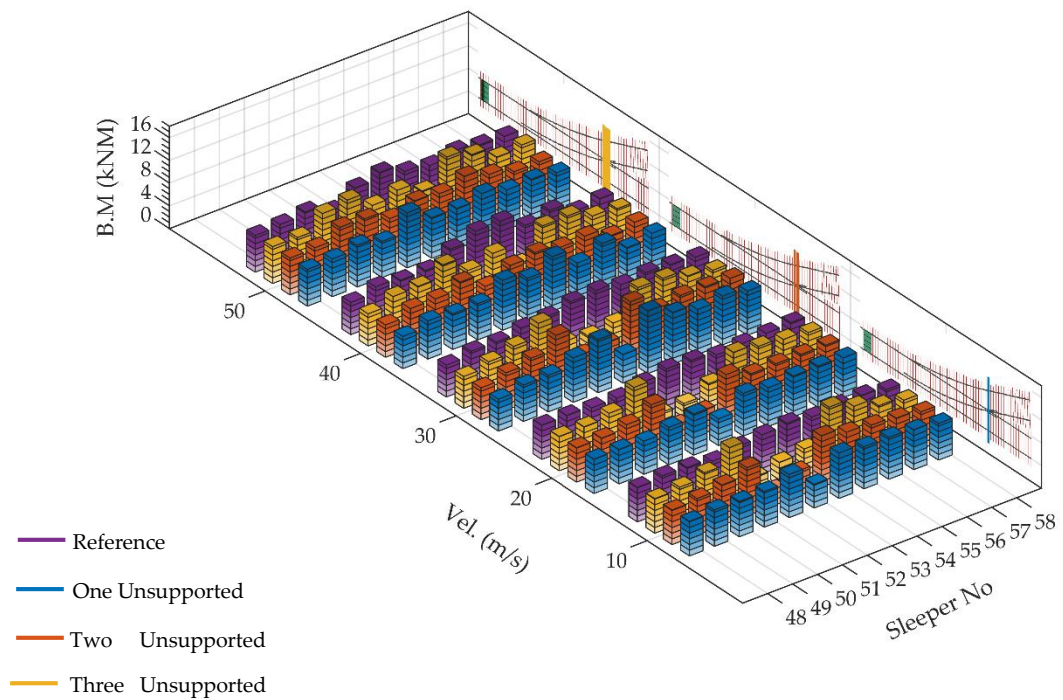


Figure 24. The distribution of positive bending moments over the bearers when unsupported bearers exist at closure panel: (a) at particular time when the front wheel is on the bearer with number 37; (b) when maximum occurs at each bearer.



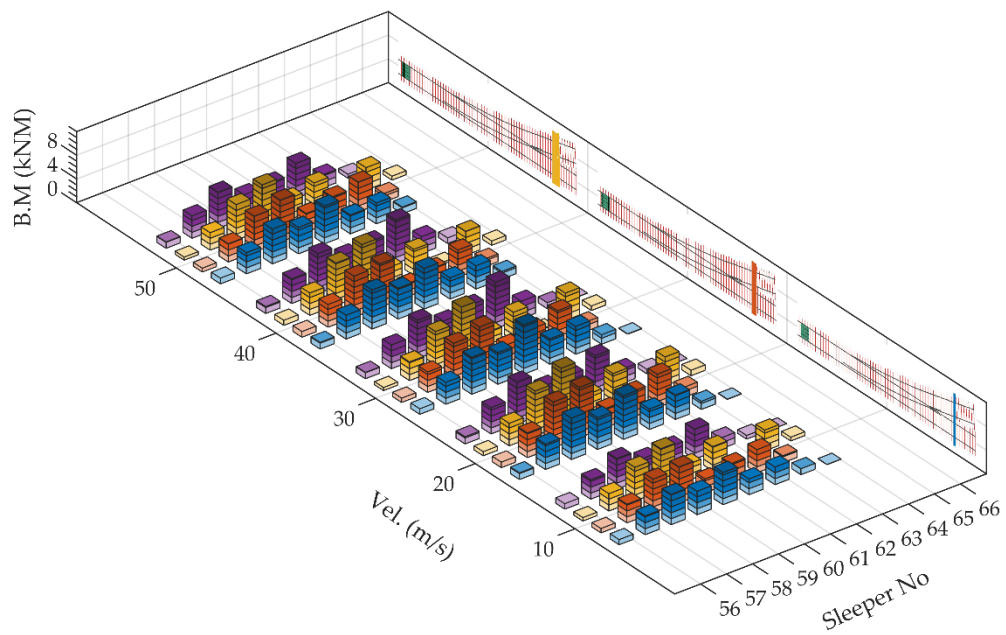
(a)



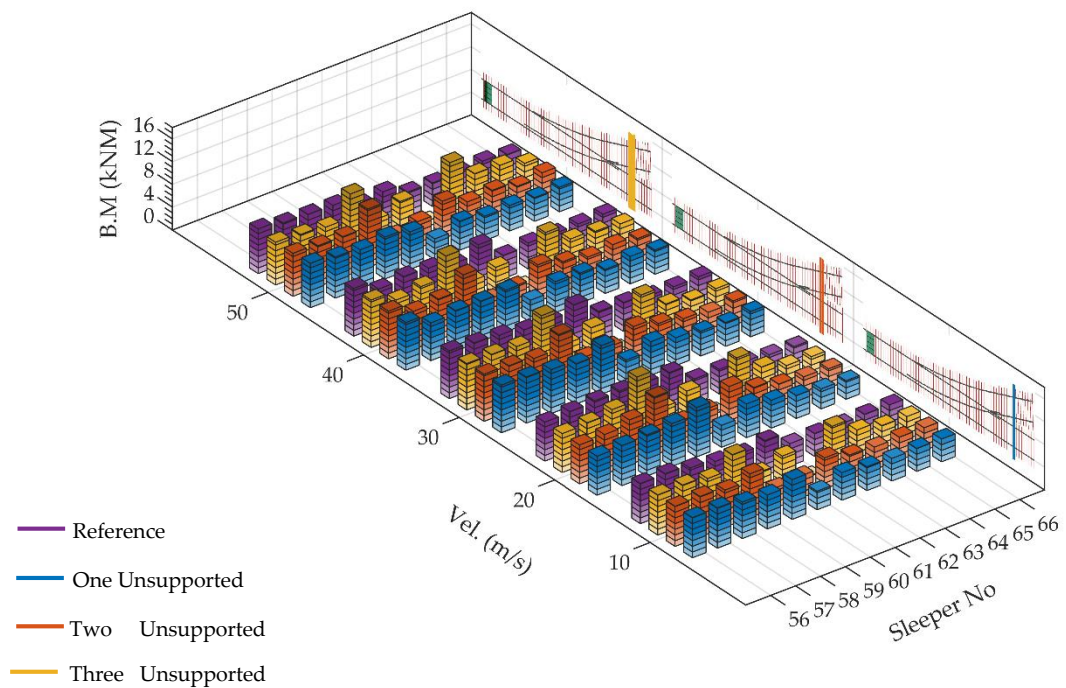
(b)



Figure 25. The distribution of positive bending moments over the bearers when unsupported bearers exist under crossing nose: (a) at particular time when the front wheel is on the bearer with number 53; (b) when maximum occurs at each bearer.



(a)



(b)

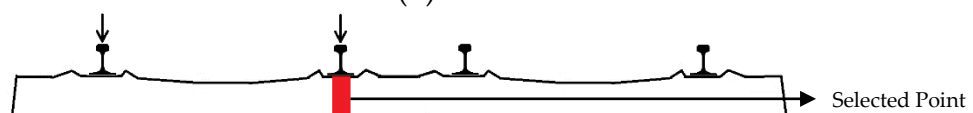
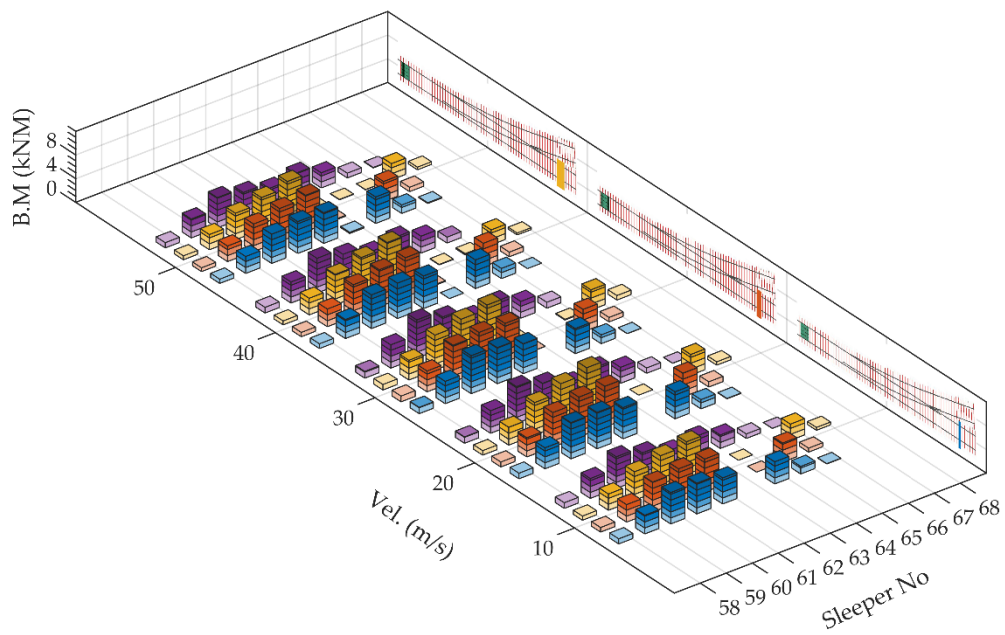
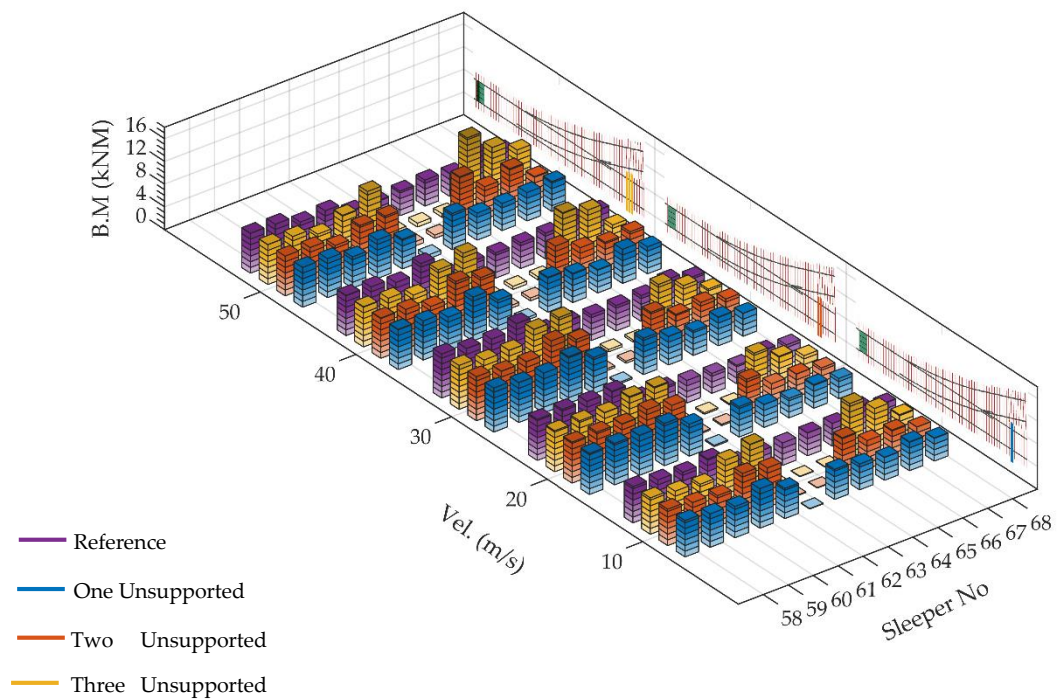


Figure 26. The distribution of positive bending moments over the bearers when the longest bearer is unsupported: (a) at particular time when the front wheel is on the bearer with number 61; (b) when maximum occurs at each bearer.



(a)



(b)

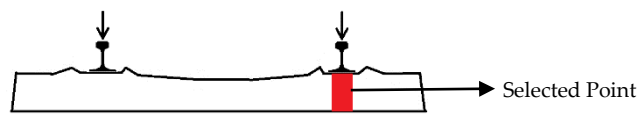


Figure 27. The distribution of positive bending moments over the bearers when the shortest bearer is unsupported: (a) at particular time when the front wheel is on the bearer with number 62; (b) when maximum occurs at each bearer.

3.6. Bending Moment Distributions Along a Bearer

The redistribution of bending moments along bearers provides better insight on how the bearers are forced. In this section, the bending moment distributions will be presented for adjacent and unsupported bearers in the case of one unsupported bearer. Other cases are omitted as they carry similar characteristic distribution with different magnitudes of bending moments. It should also be noted that graphs are plotted when the minimum and maximum bending moments occur in the middle of the track, shown in previous sections. In other words, positive bending moments in the figure could not be maximum positive moment for those particular bearers.

What is shown until this point indicates that unsupported bearers could carry significant track loads due to geometry of turnout that creates new support conditions along a bearer. The effect of idle rails that act like a support is significant and could be seen in Figures 28 and 29, where bending moment distributions of unsupported and adjacent bearers with various speeds are illustrated. As can be seen from Figure 28a, where the bending moment distribution of the unsupported bearer at entrance panel is depicted, there is no idle rail supporting the track and consequently, the force transferred to bearer is minimal, which produce a small bending moments. The magnitude of the positive and negative bending moments is approximately 1 kNm. Furthermore, the unsupported shortest bearer, which is placed at the end of turnout and illustrated in Figure 28f, exhibits similar behavior. On the other hand, the unsupported bearer under switch blades in Figure 28b reflects the contribution of the idle rail, here the open switch blade, which introduces a new support condition over the bearer. The new support causes highest negative bending moment with a value of 2.9 kNm and the positive bending moments up to 0.3 kNm at the selected point.

Among the graphs in Figure 28, the most striking is that of the bending moment distribution for the unsupported bearer under the crossing nose (Figure 28d). The figure shows that the discrepancy between positive and negative bending moments of the selected point could be imperative and reach over 5.6 kNm, in which maximum negative and positive bending moments are 2.1 kNm and 3.6 kNm, respectively. Actually, it can be seen from Figure 28d that negative and positive bending moments could also be high for the other sections of the bearer, such as the section in the middle of track in the diverging route in comparison with the selected point.

The effect of impact forces on bearers under crossing nose becomes more evident with investigation of bending moment distributions of other bearers. For instance, in Figure 28c, although the maximum negative bending moment for the selected point on the bearer at closure panel is the highest with a magnitude of 6 kNm, it has only positive bending moment of 0.4 kNm at the selected point. Despite higher level of bending moment difference, the one under the crossing nose is expected to be damaged earlier in terms of fatigue failure due to asymmetrical loadings. Moreover, the bending moment difference for the unsupported longest bearer seems to be inconsequential, which could be seen from Figure 28e. Maximum positive and negative bending moments for the selected point are 1.8 kNm and 0.5 kNm, respectively. The reason for such a low negative bending moment is that two tracks are relatively independent from each other, resulting in different support conditions. The track in the through route is supported by the rails in the diverging route. As a consequence, the inside rails produce maximum negative and positive moments when vehicle pass the unsupported bearer.

In Figure 29, the bending moment distributions of adjacent bearers to unsupported bearers are presented based on the selected point on the bearer. It is apparent from the figure that support role of the ballast bed is the origin of positive bending moment at rail seats and negative bending moment at selected points. Furthermore, it provides damping and prevents positive bending moments of the selected point. In all of the graphs, the positive bending moments of the selected points are insignificant. This might be the advantage of using FFU sleepers since the response of the system is lower compared to case with concrete sleepers that are discussed in next section.

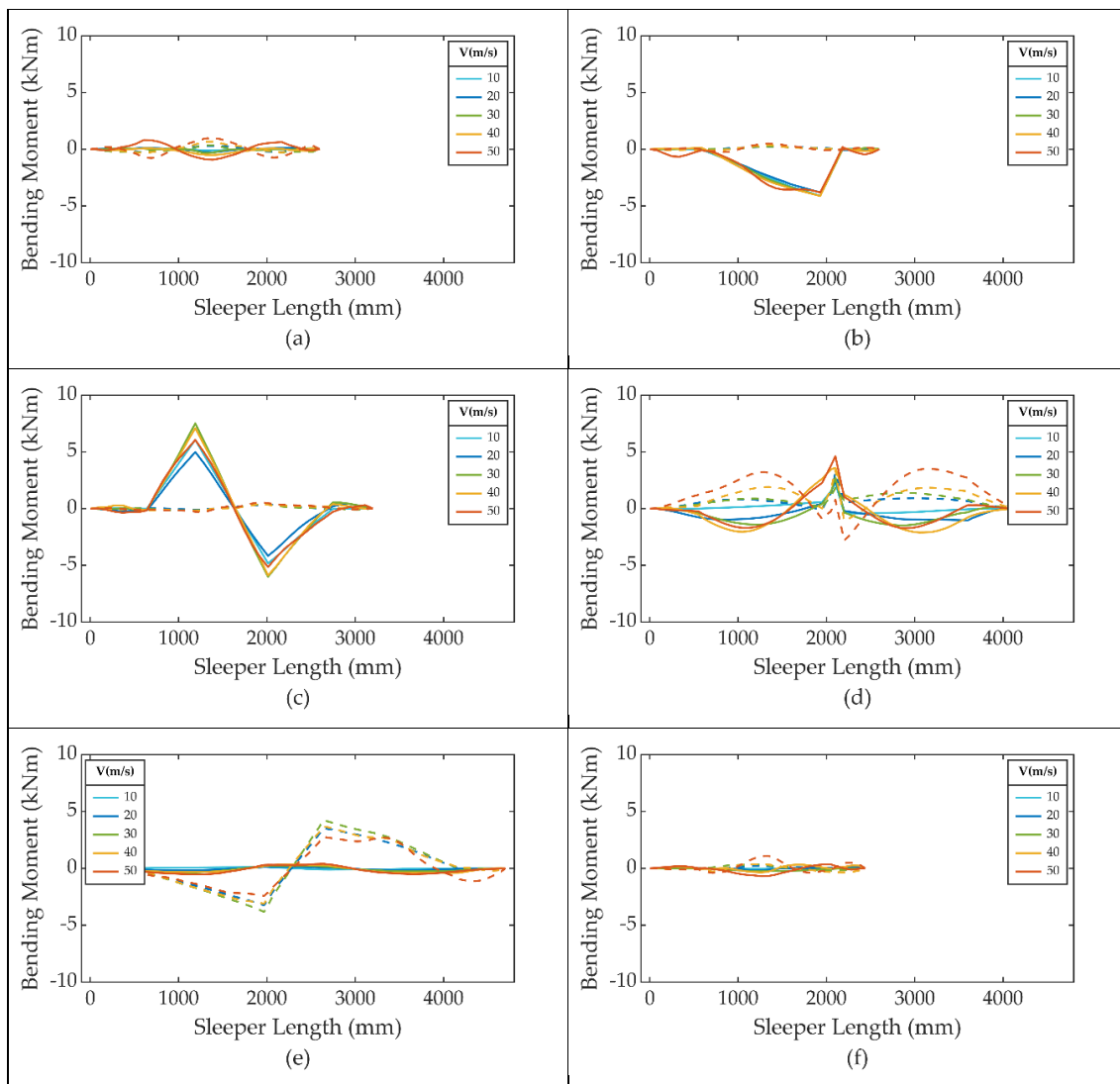


Figure 28. The flexural responses of unsupported bearers when the selected point have maximum and minimum bending moments: (a) Bearer at normal track section; (b) Bearer under switch blades; (c) Bearer at closure panel; (d) Bearer under crossing nose; (e) The longest bearer; (f) The shortest bearer.

In general, the graphs in Figure 29 show similar behavior in fully supported bearer case [12,28–31]. Symmetrical distribution in some bearers, such as bearers at normal track section or asymmetrical distributions in some bearers such as bearers at closure panel, could be observed. It is also noteworthy that the graphs are plotted for the specific point in a specific time, which means the graphs could exhibit a different profile under different selection criteria. Considering this fact, it could be concluded that comments on bending moment distributions are challenging in dynamic simulations. Nevertheless, the figures presented here give significant details on dynamic behaviors of turnout bearers.

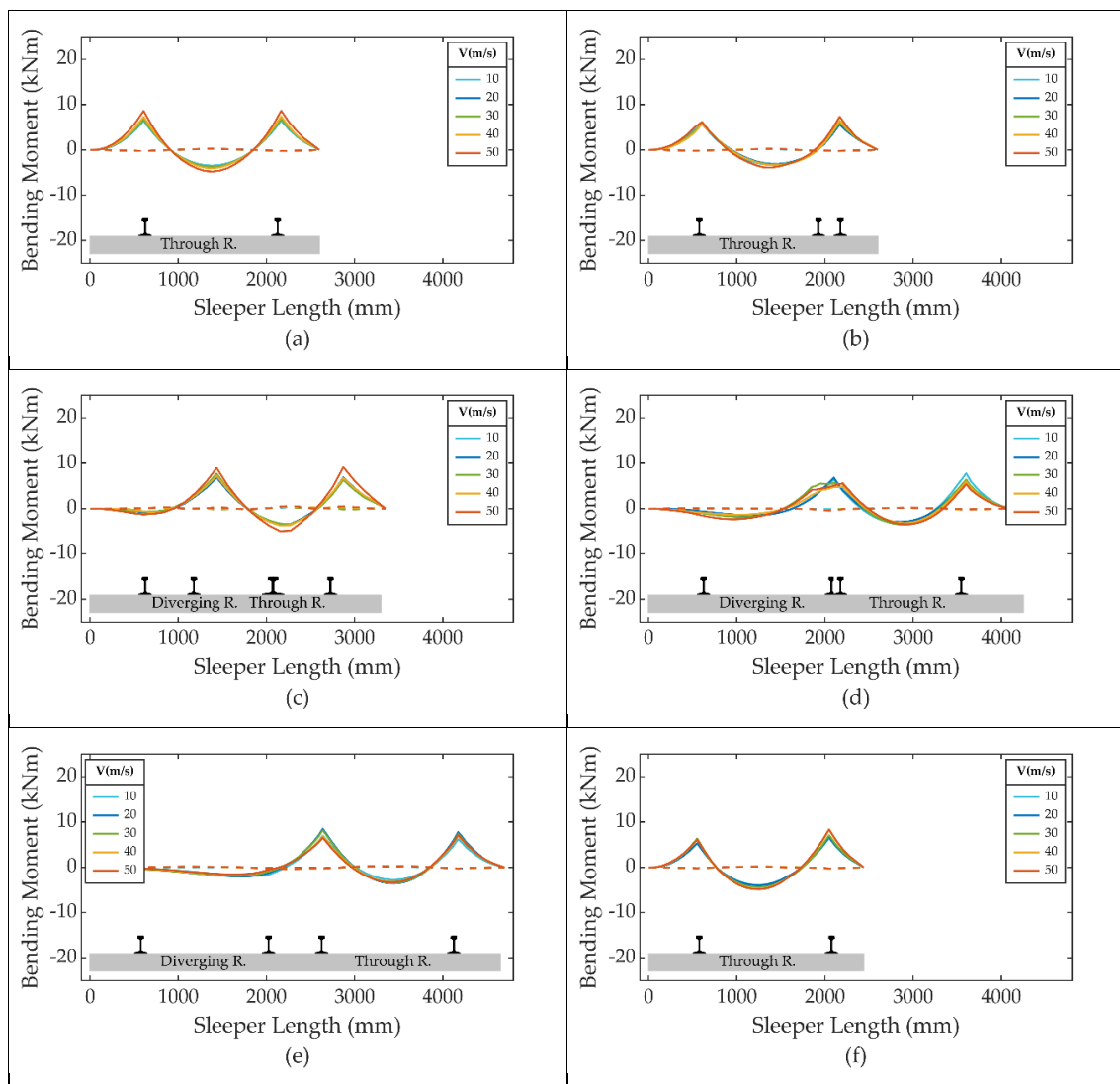


Figure 29. The flexural responses of adjacent bearers when the selected point have maximum and minimum bending moments: (a) Bearer at normal track section; (b) Bearer under switch blades; (c) Bearer at closure panel; (d) Bearer under crossing nose; (e) The longest bearer; (f) The shortest bearer.

3.7. Comparison between FFU and Concrete Sleepers

In previous sections, the positive effect of unsupported FFU bearers is observed, particularly at crossing nose. This behavior was unexpected since high impact forces emerge at this section (Figure 2). Thus, it is believed that a comparison between FFU and concrete bearers could address the positive effect. In Figures 30 and 31, the maximum bending moments of FFU and concrete bearers are plotted when one bearer under crossing nose is unsupported. As can be seen from both figures, FFU sleepers enhance the performance of the turnout in terms of positive and negative bending moments. It provides smooth transitions between turnout panels such that the maximum positive bending moment at closure panel is approximately 28% higher than maximum positive bending moment at the normal track section where as it is 80% for concrete bearers. Moreover, FFU bearers seem to be insensitive to variations in the velocity. Bending moment fluctuations, which are the result of track surface irregularities, are limited in comparison to concrete bearers, as clearly seen in the figures. Lastly, figures show that impact forces produce significant positive and negative bending moments when concrete bearers are used, despite the existing unsupported sleeper. This behavior is not observed for FFU bearers due to the positive effect of unsupported sleeper.

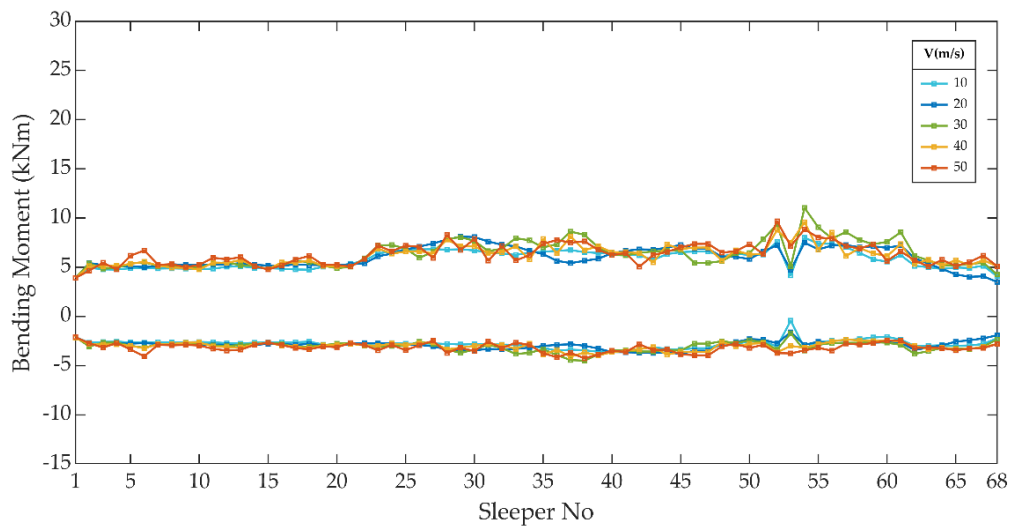


Figure 30. Maximum bending moments of the FFU bearers when one bearer under crossing nose is unsupported.

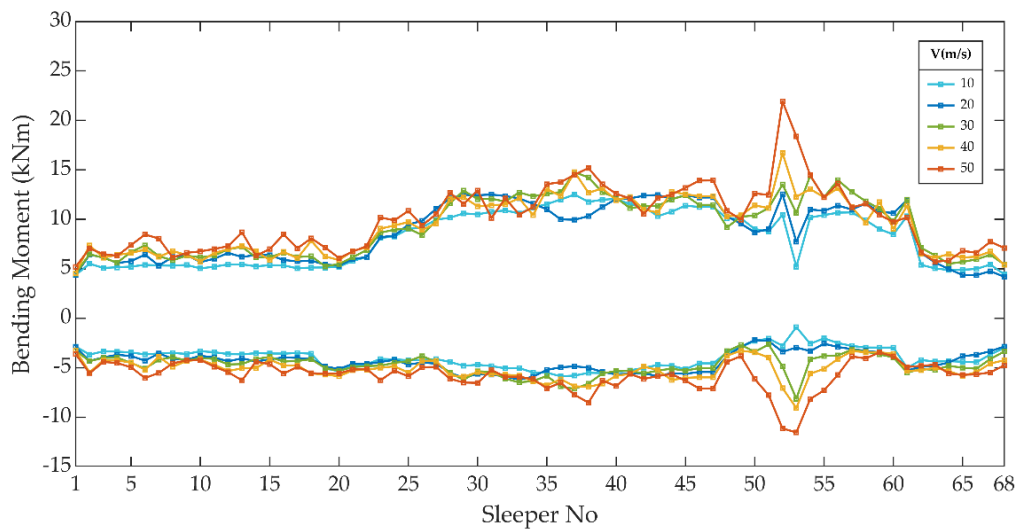


Figure 31. Maximum bending moments of the concrete bearers when one bearer under the crossing nose is unsupported.

4. Conclusions

The dynamic behavior of a turnout system that is assumed to have unsupported bearers in different locations has been investigated by numerical simulations. A numerical model of such a turnout is inherited from another numerical model that was developed previously to investigate the dynamic behavior of a turnout system. The model is capable of capturing impact forces as well as dynamic forces due to track irregularities and validated by field measurements. In the study, that model is adapted for three different unsupported cases at six different locations, and five different vehicle velocities.

The results show that the dynamic response of the turnout system with unsupported bearers exhibit exceptional behavior as opposed to the normal railway track. The complex geometry of turnout imposes different support conditions, which results in significant loads on unsupported bearers in some cases. Furthermore, bearers subjected to high frequency high magnitude impact forces are significantly forced in two directions, which increase the likelihood of the fatigue on top and bottom surfaces of the bearers.

The common findings for normal tracks in the literature are also observed in this study. An expansion of unsupported bearers increases the load distribution over the adjacent bearers. Nevertheless, bearers in different cases have been influenced differently. For instance, most affected adjacent bearers from load distribution owing to unsupported bearers are shortest bearers. They could be exposed to 2 times higher loads than the reference case. By contrast, the adjacent bearers at closure panel have more effective distribution property and so, they are subjected to lower rail seat loads. Another common finding is that higher velocities amplify the response of the system. In some cases, the amplification factor could be meaningless in comparison to reference case. For instance, the positive bending moments of the bearers at closure panel shows slight difference with respect to reference case. On the other hand, the effect of different velocities is obvious for the bearers under crossing nose.

In conclusion, the study provides new findings that could help the industry to consider the new approaches while designing, manufacturing and maintaining the bearers. It should be noted that there are several assumptions during simulations and post processing such as selecting a specific point on the bearer based on normal track experience. Those assumptions are to make comments on the phenomenon and facilitate the solution process; and also limitations in both numerical modeling and post processing process. As a consequence, further studies could be considered to find out the optimal position on the bearers for investigating dynamic behavior of turnouts.

Author Contributions: Conceptualization, M.H. and S.K., M.S.; methodology, M.H. and S.K.; software, M.H., M.S.; validation, M.H., S.K. and M.P., M.S.; formal analysis, M.H.; investigation, M.H. and S.K.; resources, S.K.; data curation, M.H.; writing—original draft preparation, M.H.; writing—review and editing, S.K. and M.P., M.S.; visualization, M.H.; supervision, S.K.; project administration, S.K.; funding acquisition, S.K. All authors have read and agreed to the published version of the manuscript.

Funding: This research was funded by European Commission, grant numbers: H2020-MSCA-RISE No. 691135 and H2020-S2R No. 730849. The APC was funded by MDPI's Invited Paper Program.

Acknowledgments: Special thanks to European Commission for H2020-MSCA-RISE Project No. 691135 "RISEN: Rail Infrastructure Systems Engineering Network" (www.risen2rail.eu) [32]. Partial support from H2020 Shift2Rail Project No 730849 (S-Code) is acknowledged. In addition, the sponsorships and assistance from Ministry of National Education (Turkey), Network Rail, RSSB (Rail Safety and Standard Board, UK) are highly appreciated.

Conflicts of Interest: The authors declare no conflicts of interest.

References

1. Grassie, S.; Cox, S. The dynamic response of railway track with unsupported sleepers. *Proc. Inst. Mech. Eng. Part D Transp. Eng.* **1985**, *199*, 123–136. [[CrossRef](#)]
2. Kaewunruen, S.; Remennikov, A. Investigation of free vibrations of voided concrete sleepers in railway track system. *Proc. Inst. Mech. Eng. Part F J. Rail Rapid Transit* **2007**, *221*, 495–507. [[CrossRef](#)]
3. Nielsen, J.C.; Igeland, A. Vertical dynamic interaction between train and track influence of wheel and track imperfections. *J. Sound Vib.* **1995**, *187*, 825–839. [[CrossRef](#)]
4. Zhu, J.; Thompson, D.; Jones, C. On the effect of unsupported sleepers on the dynamic behaviour of a railway track. *Veh. Syst. Dyn.* **2011**, *49*, 1389–1408. [[CrossRef](#)]
5. Lundqvist, A.; Dahlberg, T. Load impact on railway track due to unsupported sleepers. *Proc. Inst. Mech. Eng. Part F J. Rail Rapid Transit* **2005**, *219*, 67–77. [[CrossRef](#)]
6. Zhang, S.; Xiao, X.; Wen, Z.; Jin, X. Effect of unsupported sleepers on wheel/rail normal load. *Soil Dyn. Earthq. Eng.* **2008**, *28*, 662–673. [[CrossRef](#)]
7. Zhu, J.J.; Ahmed, A.; Rakheja, S.; Khajepour, A. Development of a vehicle–track model assembly and numerical method for simulation of wheel–rail dynamic interaction due to unsupported sleepers. *Veh. Syst. Dyn.* **2010**, *48*, 1535–1552. [[CrossRef](#)]
8. Zakeri, J.A.; Fattahi, M.; Ghanimoghadam, M.M. Influence of unsupported and partially supported sleepers on dynamic responses of train–track interaction. *J. Mech. Sci. Technol.* **2015**, *29*, 2289–2295. [[CrossRef](#)]
9. Mosayebi, S.-A.; Zakeri, J.A.; Esmaeili, M. Effects of train bogie patterns on the mechanical performance of ballasted railway tracks with unsupported sleepers. *Proc. Inst. Mech. Eng. Part F J. Rail Rapid Transit* **2018**, *232*, 238–248. [[CrossRef](#)]

10. Kaewunruen, S.; Remennikov, A.M.; Dindar, S. Influence of Asymmetrical Topology on Structural Behaviours of Bearers and Sleepers in Turnout Switches and Crossings. In *Sustainable Civil Infrastructures, Proceedings of the International Congress and Exhibition "Sustainable Civil Infrastructures: Innovative Infrastructure Geotechnology"*; Springer: Cham, Switzerland, 2017; pp. 51–60.
11. Kaewunruen, S.; Ngamkhanong, C.; Janeliukstis, R.; You, R. Dynamic amplification factors for railway turnout bearers in switches and crossings. In Proceedings of the 6th ECCOMAS Thematic Conference on Computational Methods in Structural Dynamics and Earthquake Engineering (CompDyn2017), Rhodes Island, Greece, 15–17 June 2017; pp. 15–17.
12. Hamarat, M.; Kaewunruen, S.; Papaalias, M.; Silvast, M. New Insights from Multibody Dynamic Analyses of a Turnout System under Impact Loads. *Appl. Sci.* **2019**, *9*, 4080. [[CrossRef](#)]
13. Kaewunruen, S. In situ performance of a complex urban turnout grillage system using fibre-reinforced foamed urethane (FFU) bearers. In Proceedings of the 10th World Congress on Rail Research, Sydney, Australia, 24–27 November 2013; pp. 25–28.
14. Kaewunruen, S. Acoustic and dynamic characteristics of a complex urban turnout using fibre-reinforced foamed urethane (FFU) bearers. In *Noise and Vibration Mitigation for Rail Transportation Systems*; Springer: Berlin/Heidelberg, Germany, 2015; pp. 377–384.
15. Kaewunruen, S. Monitoring in-service performance of fibre-reinforced foamed urethane sleepers/bearers in railway urban turnout systems. *Struct. Monit. Maint.* **2014**, *1*, 131. [[CrossRef](#)]
16. Kaewunruen, S.; Remennikov, A. *Dynamic Properties of Railway Track and Its Components: A State-Of-The-Art Review*; Nova Science Publishers: New York, NY, USA, 2008.
17. RRSB. *Signing of Permissible Speeds and Speed Restrictions*; Safety & Standards Directorate Railtrack PLC: London, UK, 2000.
18. Esveld, C. *Modern Railway Track*, 2nd ed.; Delft University of Technology: Zaltbommel, The Netherlands, 2001.
19. Hallquist, J.O. LS-DYNA keyword user's manual. *Livermore Softw. Technol. Corp.* **2007**, *970*, 299–800.
20. Kaewunruen, S.; Xie, L.; Goto, K. Damping characteristics of composite sleepers and bearers in railway switches and crossings. In Proceedings of the 26th International Congress on Sound and Vibration, Montreal, QC, Canada, 7 July 2019.
21. Sengsri, P.; Oliveira De Melo, A.; Kaewunruen, S. Experimental and numerical investigation of vibration characteristics of fibre-reinforced foamed urethane composite beam. In Proceedings of the 4th World Multidisciplinary Civil Engineering-Architecture-Urban Planning Symposium, Prague, Czech Republic, 17–21 June 2019.
22. De Man, A. Pin-pin resonance as a reference in determining ballasted railway track vibration behaviour. *Heron Engl. Ed.* **2000**, *45*, 35–52.
23. Goto, K.; Minoura, S.; Watanabe, T.; Ngamkhanong, C.; Kaewunruen, S. Impact Load Response of PC Rail Joint Sleeper under a Passing Train. *J. Phys. Conf. Ser.* **2018**, *1106*, 012008. [[CrossRef](#)]
24. Setsobhonkul, S.; Kaewunruen, S.; Sussman, J.M. Lifecycle Assessments of Railway Bridge Transitions Exposed to Extreme Climate Events. *Front. Built Environ.* **2017**, *3*, 35. [[CrossRef](#)]
25. Kaewunruen, S.; Remennikov, A.M. Current state of practice in railway track vibration isolation: An Australian overview. *Aust. J. Civ. Eng.* **2016**, *14*, 63–71. [[CrossRef](#)]
26. Kaewunruen, S.; Remennikov, A.M. Experiments into impact behaviour of railway prestressed concrete sleepers. *Eng. Fail. Anal.* **2011**, *18*, 2305–2315. [[CrossRef](#)]
27. Kaewunruen, S.; Remennikov, A.M.; Murray, M.H. Introducing a new limit states design concept to railway concrete sleepers: an Australian experience. *Front. Mater.* **2014**, *1*, 8. [[CrossRef](#)]
28. Kaewunruen, S.; Ishida, T.; Remennikov, A.M. Dynamic performance of concrete turnout bearers and sleepers in railway switches and crossings. *Adv. Civ. Eng. Mater.* **2018**, *7*. [[CrossRef](#)]
29. Kaewunruen, S.; Aikawa, A.; Remennikov, A.M. The importance of 'dynamics' in the design and performance-based testing criteria for railway track components. *Procedia Struct. Integr.* **2019**, *21*, 83–90. [[CrossRef](#)]
30. Kaewunruen, S.; You, R.; Ishida, M. Composites for Timber-Replacement Bearers in Railway Switches and Crossings. *Infrastructures* **2017**, *2*, 13. [[CrossRef](#)]

31. Silva, E.A.; Pokropski, D.; You, R.; Kaewunruen, S. Comparison of structural design methods for railway composites and plastic sleepers and bearers. *Aust. J. Struct. Eng.* **2017**, *18*, 160–177. [[CrossRef](#)]
32. Kaewunruen, S.; Sussman, J.M.; Matsumoto, A. Grand challenges in transportation and transit systems. *Front. Built Environ.* **2016**, *2*, 4. [[CrossRef](#)]



© 2020 by the authors. Licensee MDPI, Basel, Switzerland. This article is an open access article distributed under the terms and conditions of the Creative Commons Attribution (CC BY) license (<http://creativecommons.org/licenses/by/4.0/>).